Unusually Quick Development of a 4000 nT Substorm During the Initial 10 Minutes of the 29 October, 2003 Magnetic Storm

M. Yamauchi[1], T. Iyemori[2], H. Frey[3], and M. Henderson[4]

1. Swedish Institute of Space Physics, Kiruna, Sweden
2. Data Analysis Center C2 for Geomagnetism and Space Magnetism, Kyoto University, Kyoto, Japan
3. Space Science Laboratory, University of California, Berkeley, CA, USA
4. Los Alamos National Lab, Los Alamos, NM, USA

Abstract

Global geomagnetic field data, IMAGE FUV data, and many other in-situ observations are presented for the initial 10 minutes of the magnetic storm starting 29 October 2003 at around 06:10 UT. Within one minute after sudden commencement (SC), two independent strong westward ionospheric electrojets (> 2000 nT) at the inner magnetospheric region started simultaneously, one in the evening-midnight sector and the other in the morning sector. Both activities expanded and accompanied auroral expansion. The locations (inner magnetosphere), morphologies (expansion), and intensities (> 2000 nT) of both activities fall into substorm expansive phases. Having such simultaneous independent 2000 nT level expansions makes this event unique. The interplanetary magnetic field condition before the SC was not favorable in causing an AL<-2000 nT activity. A timing analyses indicates that these strong westward electrojets were most likely triggered by the interplanetary shock, with the triggering location not farther than the geosynchronous distance. They are also probably maintained by the direct energy pumping from the solar wind because cross-tail current derived from the closely located GOES-10 and Polar did not decrease very much during this period. A local but even stronger geomagnetic (nearly 4000 nT) and auroral activity started only 6 minutes after the start of SC at post-midnight where and when the above two expanding activities met each other, although the relation between the onset of 4000 nT activity and the preceding expansions is not clear. The suddenness of this third activity (3000 nT change within 2 minutes) is another unique feature.

(Yamauchi, et al., J. Geophys. Res., 111(A4), A04217, doi:10.1029/2005JA011285, 2006.

Key words: 2790 Substorms, 2437 Ionospheric dynamics, 2784 Solar wind/magnetosphere interactions, 2409 Current systems; initial phase; magnetic storm; substorm onset.

1. INTRODUCTION

Major magnetic storms normally start with sudden commencement (SC: a sudden increase in geomagnetic field or the Dst index at dayside stations due to the compression of the magnetosphere) followed by a quick development of large negative changes in the Dst index toward its negative peak within several hours, and a long decay of Dst decrease which takes a few to several days. At high latitudes, large substorms take place shortly after the SCs, with typical delay time of tens of minutes from the initial rise of SC before the onset of the substorm expansive phase. The geomagnetic activity related to the substorm expansive phase normally propagates from the nightside to the dayside.

This is the standard view right after large SCs [e.g., Chapman and Bartels, 1940], and individual storms can deviate from this. Some SCs are followed by substorm onsets only several minutes after [Akasofu and Chapman 1972]. Here we use the term "substorm" in the classic sense [Akasofu, 1964], i.e., a combination of large-scale phenomena lasting tens of minutes: sudden auroral brightening, its poleward expansion, and simultaneous sudden decrease of horizontal component of the ground geomagnetic field more than 500 nT caused by a strong and expanding westward electrojet. The onset of such expansion (substorm onset) takes place in the nightside sector with highest probability in the pre-midnight region, and its triggering mechanism remains a controversial issue in magnetospheric physics [see e.g., Akasofu, 2004; Ohtani, 2004; Lyons and Wang, 2004; and references therein].

%%%%%% Figure 1 %%%%%%

The large magnetic storm starting at around 06:10 UT on 29 October 2003 (see Dst in Figure 1) shows a slightly different behavior from the standard storms [Lopez et al., 2004]. For example, Dst shows three unusual peaks, indicating that the initial activity could have died away if the second period of large southward interplanetary magnetic field (IMF) not started at around 18 UT (data not shown here). The continuous activity seen in the AL index (Figure 1) between the Dst peaks might provide an important clue in understanding the storm-substorm relation [e.g., Kamide et al., 1998; Ohtani et al., 2001; and references therein] because the peaks of Dst correspond precisely to peaks of AL with extremely large values (nearly -4000 nT) and strongly southward IMF (more than -20 nT). However, we do not discuss this problem in this paper.

We here focus on the first 10 minutes after the start of SC, i.e., the initial development of the storm because of its unusual behavior. Three onsets of strong westward ionospheric Hall current (electrojet) together with auroral brightening took place within this short interval, and the activity levels of these westward electrojets are quite high, reaching 2000 nT deviations of the geomagnetic horizontal (H) component for the first

two activities within 5 minutes after the start of SC, and nearly 4000 nT for the last activity within 10 minutes after the start of SC. Such a quick and extremely large development of multiple current systems immediately after the start of SC has never been reported. We examined 10.5 years data of final AE (with error-checked calibrated data from all 12 stations) from January 1978 to June 1988, and found only 32 days of AL<-2000 nT, with none of the events registered as quickly as the present case after the start of SC. Therefore, it is important to describe the minute-to-minute development of the present activity using as many data sets as possible. This is the main purpose of this paper.

Nearly simultaneous global intensification of the aurora and the westward electrojet in response to a solar wind density increase (pressure pulse) is found during the January 1997 storm event [e.g., Shue and Kamide, 1998; Zhou and Tsurutani, 1999; Zesta el al., 2000]. Zesta el al. [2000] suggested that this activity is not a standard substorm although the observed auroral and geomagnetic signatures belong to the classic definition of the substorm expansion phase. Since the majority of the substorm models do not allow multiple onset locations of the expansive phase, it is wise to discuss this type of activity separately from the ordinary substorm. Then the question arises on what are differences and similarities between these nonstandard substorms and the standard ones. The question includes on the morphology of the substorm development (e.g., pseudo-breakup and ordinary breakup), the energy flow (loading-unloading and directly-driven problem), and the triggering mechanism.

To answer the question one has to examine as many nonstandard examples as possible because only few examples have been reported on this type of substorms onset, i.e., the nearly simultaneous global onset of the auroral intensification/expansion as the arrival of the interplanetary shock or pressure pulse including the SC. With reported few examples, the sudden auroral intensification in response to the solar wind pressure pulse show a different electron spectrum from those during the ordinary substorm [Chua et al., 2001; Boudouridis et al., 2003; Meurant et al. 2003]. However, none of the reported examples registered AL<-800 nT except for the January 1997 event that registered nearly -1500 nT of geomagnetic deviation [Shue and Kamide, 1998]. The majority of the events are auroral intensification without strong westward electrojet [Zhou et al., 2003]. Therefore, the present case provides a unique example of this type of phenomena.

We collected data from the ground-based magnetometers, IMAGE satellite (FUV), geosynchronous satellites (LANL particle and GOES magnetic field), and the ISTP satellites (field data). In section 2 we show the time sequence how the interplanetary shock passed through the interplanetary space and the magnetosphere with extremely fast propagation velocity (nearly 2000 km/s). This information is used in deriving the arrival time of the shock on the Earth, near-Earth plasma sheet (several to 10 R_E, candidate location for the current disruption [Lui, 2004; and references therein]), and

the near-Earth magnetic neutral region (10-30 R_E, candidate location for the magnetic reconnection [Nagai and Machida, 1998; Asano et al., 2004]). In section 3 we show the development of the substorms (in the classic definition mentioned above) in the ionosphere and conjugating geosynchronous orbit. These data are further discussed in terms of the timing and mapping in section 4. Timing information limits the candidate triggering location of the present nonstandard substorm, whereas the mapping relation limits the magnetospheric source of the morning activity.

2. ARRIVAL OF INTERPLANETARY SHOCK

Reliable solar wind data is not available for this event because the extremely high particle flux the day before [Lopez et al., 2004] upset the plasma instruments of SOHO, ACE, Geotail, and WIND spacecraft. Therefore, only the arrival times of the interplanetary shock obtained by the magnetometer data can provide the average propagation velocity of the shock. Below we describe the time sequence of shock propagation near the Earth with time resolutions of 10 sec or better except for ACE (with 16-seconds resolution).

%%%%%% Figure 2 %%%%%%

Figure 2 shows the IMF data observed by the ACE and Geotail spacecraft. The ACE spacecraft at 221 R_E upstream of the Earth detected the arrival of shock (increase of total |B|) at around 05:58:20 UT (16s resolution) followed by dawnward IMF (B_Y = -30 nT) for more than 10 minutes. The Geotail spacecraft at 26 R_E upstream of the Earth detected the shock at around 06:09:40 UT. From these timings, the solar wind velocity is estimated as 1900-2000 km/s and the arrival of the shock at the Earth is estimated at around 06:11 UT. In fact the WIND spacecraft detected the arrival of deformed shock or plasmoid at around 06:19:30 UT at 156 R_E downstream of the Earth (data are not shown), which is consistent with the 2000 km/s velocity.

%%%%%% Figure 3 %%%%%%

In the magnetosphere, LANL geosynchronous satellites detected the arrival of this shock at around 06:11 UT as shown in Figure 3. Figure 3a and Figure 3b show fluxes of energetic protons and electrons, respectively, from six LANL satellites in 10-seconds resolution. Two of the LANL satellites were located near noon (LANL-02A at 11 LT and LANL-97A at 13 LT) at the shock arrival and they detected sudden increase in energetic proton fluxes and short spikes in energetic electron fluxes at 06:10:50 UT. The electron spike is immediately followed by decrease in fluxes. The increase of fluxes is probably due to the shock passage. The proceeding changes of proton flux and electron flux in opposite sense suggest that the satellite went into the other region with

electron/proton ratio quite different (such as the magnetosheath or a larger L-shell region) due to the strong compression of the magnetosphere.

The sudden change in energetic particle fluxes is registered 20 sec later at 06:11:10 UT at 07 LT (LANL-01A), 30 sec later at 06:11:20 UT at 16 LT (1994-084) and 04 LT (1990-095), and 40 sec later at 06:11:30 UT at 19 LT (1991-080). The time sequence illustrates the propagation of the shock effect via both morning and evening sectors with a velocity of nearly 2000 km/s, the same as the solar wind velocity.

%%%%%% Figure 4 %%%%%%

These timings match with the shock arrival observed by GOES geosynchronous satellites at 21 LT and 01 LT as shown in Figure 4. Both GOES-10 at 225 long (thin lines) and GOES-12 at 285 long (thick lines) detected sudden stretching of magnetic field (decrease of poleward component and increase of tailward components) at around 06:11:40 UT with GOES-12 at 01 LT preceding by several seconds GOES-10 at 21 LT. Figure 4 also shows the magnetometer data from Polar satellite at 21 LT in broken lines. Its location (21 LT, or X_{GSM} = -5.3 R_E, Y_{GSM} = +4.8 R_E, Z_{GSM} = -0.7 R_E) was only 1 R_E away from GOES-10 (21 LT, or X_{GSM} = -5.1 R_E, Y_{GSM} = +4.0 R_E, Z_{GSM} = -1.5 R_E) at this particular time. Polar detected the shock arrival at 06:11:30 UT.

Magnetometer data from Cluster (not shown here), which was located in the southern lobe (Z=-10 R_E, X=0 R_E), also detected the arrival of the shock at around 06:11:20 UT in 10s resolution [Tim Horbury, private communication, 2005]. This is the same timing as that detected by the LANL geosynchronous satellite at 16 LT. Both the Cluster and Polar spacecraft registered increases of 10 keV range ions with 10 to 20 sec delay from the magnetic signature, and in this sense the arrival times of shock at LANL satellites could be slightly (few to 10 sec) earlier than those described above, but this is not very essential.

%%%%%% Figure 5 %%%%%%

The arrival of the shock, or the SC, is recognized in SYM-H starting at 06:11 UT with one-minute resolution in Figure 1 (bottom panel). For higher time resolution, Figure 5 shows 1s-resolution geomagnetic field data at the Kiruna (07 LT, 65° GMLat), Urumqi (12 LT, 34° GMLat), Memanmetsu (16 LT, 35° GMLat), and Kanoya (15 LT, 22° GMLat) stations between 06:11:00-06:11:30 UT (30 sec data). All stations registered the start of the SC-associated ΔH (horizontal component) at 06:11:21 UT (this means 06:11:30 UT in 10s resolution, and 0611 UT in one-minute resolution as is recognized in SYM-H in Figure 1). The simultaneous arrival time is not very surprising if one considers the cavity mode propagation, i.e., electromagnetic wave propagation in the Earth-ionosphere waveguide [Araki et al., 1997]. A magnetic signal may propagate with the speed of light in the non-conducting atmosphere sandwiched by the conducting

ground and ionosphere. On the other hand, the sweeping velocity of the shock in the magnetosphere at around 0.3 R_E/s is also consistent with the nearly simultaneous arrival time in this particular case.

%%%%%% Figure 6 %%%%%%

Figure 6 summarizes how the interplanetary shock traveled. The arrival time is quite ordered from upstream to downstream with a velocity of 2000 km/s for both outside and inside the magnetosphere. This suggests that the shock simply swept from the upstream to the downstream rather than along the magnetic field. Such a simple propagation sometimes happens for large SCs [e.g., Petrinec et al., 1996]. The consistent propagation velocity throughout the upstream interplanetary space, the magnetosphere, and the downstream interplanetary space (≈0.3 R_E/s) allows us to estimate the arrival time of the shock in 10-seconds accuracy in the near-Earth tail where no satellite was located.

3. SUBSTORM DEVELOPMENT

In this section we examine the minute-to-minute development of the geomagnetic and auroral activities during the initial 10 minutes from the start of SC. We examine the worldwide ground-based magnetometer data, geostationary satellite data, and the optical data from the IMAGE satellite. The actual geomagnetic disturbance is larger than what is indicated by AL with a more complicated sequence. SYM-H (which is equivalent to Dst) is positive during this period as shown in Figure 1, and in this sense it is during the initial (compression) phase of the magnetic storm.

3.1. GEOMAGNETIC DISTURBANCES

Immediately following the start of SC at around 06:11:20 UT, both the ASY-H and ASY-D indices started to deviate at 06:12 UT as shown in Figure 1, indicating a development of the ionospheric current (note that the effect of the field-aligned current and the Pedersen current are mostly cancelled out). At high latitudes, the AU index shows the SC amplitude of > +1000 nT at 06:12 UT, and this is immediately followed by a large development of negative AU and AL. Although AL and AU in Figure 1 are provisional ones derived from limited stations (coverage is only over the nightside from evening to late morning at 6 UT) without data qualification, these large-scale variations are real. Thus, the ionospheric current system has started to develop immediately after the shock arrival. Let us examine this in more detail by looking at data from individual stations.

%%%%%% Figure 7 %%%%%%

Figure 7 shows geomagnetic X (or H) component at ground stations all over the world during 06:00-06:30 UT on 2003-10-29. Resolution is one minute (60-seconds averages around the turning of minutes, i.e., average from 30th second to 29th second) except Kiruna (KRN) at the bottom of Figure 7a that is in 1-second resolution. Figure 7a shows data at stations in the auroral zone (magnetic latitude is around 62-70 GMLat), Figure 7b shows data at stations equatorward (magnetic latitude <62 GMLat), and Figure 7c shows data at stations poleward (magnetic latitude >71 GMLat).

During this period the geomagnetic north pole was located in the local midnight (23-0 LT). This fact made the actual dipole tilt angle about 22~23 degrees with respect to the solar wind during this short period. Such a tilt may cause an inter-hemispheric asymmetry on the electric current system due to, e.g., mapping configuration of the geomagnetic field and the conductivity difference. In fact, a strong inter-hemispheric asymmetry is recognized in the geomagnetic disturbances, i.e., between the AIA station (296 long and -55 GMLat) and the OTT station (284 long and +56 GMLat) although both stations are located in the midnight sector. Therefore, it is wise to first examine mainly the data from the northern hemisphere where we have much better coverage of the ground station than the other hemisphere, and later consider the inter-hemispheric relation where such examination is useful.

The SC is registered at 06:11 UT or 06:12 UT at most of the stations. In KRN's 1-second resolution data, the peak value is as high as $\Delta Bx = +450$ nT registered at 06:12:02 UT. Right after the SC recognition, a large negative bay of ΔBx started at high latitudes during the initial (compression) phase, i.e., when SYM-H is positive. In the 1-second resolution data at the KRN station, ΔBx is more than -500 nT within 60 sec, and -1000 nT within 6 minutes after the SC peak. Similarly, large negative deviations of ΔBx were recognized in other stations immediately after the SC peak. At already 06:13 UT when KRN registered -500 nT, many other stations also registered -500 nT deviations in the one-minute average values, including the evening-midnight (CMO, YKC, PBQ) and the morning (SOD, ABK, LRV) stations. The largest deviations at that time are registered at CMO (212 long), PBQ (282 long) and LRV (338 long) in the auroral zone (Figure 7a).

The timing of the onset of the evening-midnight activity is estimated to be 06:12 UT in one-minute resolution, as is seen at the CMO, MEA (247 long) and PBQ stations. This onset timing is also valid in the southern hemisphere as is seen at the AIA station which shows a 500 nT change from 06:12 UT. The negative ΔBx deviation at 06:12 UT at many other evening-midnight stations could be either the onset of the activity or a part of the SC signal.

The large ΔBx deviation registered at the midnight PBQ station (1500 nT at 06:15 UT and 2000 nT at 06:16 UT) is interpreted as a part of the evening-midnight activity (seen at around 65 GMLat) because the stations just a few degrees north (BRW, YKC, and

FCC) consistently detected the same smooth development with a few minutes delay. The ΔBx deviation at all pre-midnight stations reached their peaks at 06:16-06:18 UT and quickly decayed afterward. Limiting the data from the latitude range 68-69 GMLat, ΔBx at YKC (246 long) reached the peak earlier than FCC (266 long) or BRW (203 long).

On the other hand, large ΔBx deviation in the morning sector shows a different development from those of the evening sector. For example, ΔBx variation at the LRV (338 long), LER (359 long), and LOV (18 long) stations shows step-like change between 06:11-06:14 UT with sustained activity after the peak, and this is quite different from the smooth one-peak ΔBx variation at the pre-midnight stations mentioned above. Thus, the ΔBx development in the morning sector is most likely independent of that in the evening-midnight sector. A similar independency is also found in both the sub-auroral region and the polar cap.

Furthermore, the amplitude of ΔBx at LRV is larger than that of NAQ or FCC (they are located west of LRV) at the same latitude until 06:17 UT, and is even larger than that of PBQ until 06:16 UT (2000 nT already at 06:15 UT). Such separation is also seen outside the auroral region. The ΔBx deviation is larger at late morning than at early morning both in the sub-auroral region (e.g., LOV and NUR) with negative ΔBx and in the polar cap (e.g., BJN) with positive ΔBx during 06:12-06:14 UT. We see the minimum of the activity at NAQ (315 long) in the auroral region, and STJ (307 long) and VAL (350 long) in the sub-auroral region. Therefore, there is an extra kernel of activity in the morning sector at around 04 LT (corresponding to 05~06 MLT). The independence of the morning activity is also seen in IMAGE satellite data (see section 3.3). Therefore, although the longitudinal coverage of the geomagnetic stations is not dense enough to give a concrete picture, the double-location (morning and evening) of the enhancement is not an artifact of the finite number of the geomagnetic stations.

The onset time of the morning activity is no later than 06:13 UT, i.e., at the next data point after the SC is recognized. Some sub-auroral stations (e.g., BFE and NUR) show ΔBx as large as 100 nT already at 06:12 UT, but we cannot separate the SC effect from this ΔBx deviation. During the first 5 minutes after the start of SC, all the morning stations in Figure 7 showed stepwise but steady development of ΔBx except for an overshoot at 06:13 UT in northern Scandinavia (TRO, ABK≈KRN, and SOD). Such a monotonic large-scale development indicates an expansion of an active region if one looks at the number of stations that registered ΔBx < -500 nT. For example NAQ (315 long) registered ΔBx < -500 nT two minutes after LRV (338 long) at the same latitude. In this respect, the expansion is seen in the latitudinal direction for the evening-midnight activity, and in the longitudinal direction (anti-sunward) for the morning activity. Such a quick large-scale response with large amplitudes is not very common at this local time.

These large negative deviations of ΔBx in the morning sector are not the signature of the compression because compression should cause a positive ΔBx instead. In fact a positive spike of ΔBx is recognized in the KRN 1-second resolution data in Figure 7a. It is also different from the signature of an anti-sunward (poleward on the ground) traveling vortex [e.g., Friis-Christensen et al., 1988]. We do not recognize any traveling bipolar signatures, but a large-amplitude standing PC-5 pulsation (signature of oscillation of the geomagnetic field line), in the Norwegian magnetometer chain at 07 LT (not shown here) as well as the Greenland magnetometer chain at 03 LT [J. Watermann, private communication, 2005]. The intensity of 2000 nT at the LRV station can hardly be explained by the vortex. Therefore, the data right after the start of SC is interpreted as an instantaneous development of a strong westward ionospheric electrojet in the morning sector. A westward electrojet in the morning sector means a sunward convection, and is not directly pushed by the solar wind but rather driven by the increasing ionospheric electric field, or equivalently the magnetosphere-ionosphere current system.

In addition to the westward electrojet, one can recognize at the BJN (71 GMLat) and HRN (74 GMLat) stations a large positive ΔBx, i.e., eastward electrojet (or anti-sunward convection). The Norwegian magnetometer chain at 07 LT (not shown here) shows that a convection reversal at around 68-69 GMLat started to develop already at 06:13 UT, i.e., at the next data point after the SC was recognized. The pair of westward and eastward electrojets (or sunward and anti-sunward convection) indicates a development of a current system with three field-aligned currents. One is "downward" current from the magnetosphere into the ionosphere at around the convection reversal (67-71 GMLat), and the others are "upward" currents from the ionosphere to the magnetosphere at the low-latitude boundary of the westward electrojet and at the high-latitude boundary of the eastward electrojet. The downward current at around the convection reversal in the morning sector is traditionally called the Region 1 current in both hemispheres [Iijima and Potemra, 1976; Friis-Christensen et al., 1985; Potemra 1994 and references therein], and normally flows inside the low-latitude boundary layer [Woch et al., 1993]. While the upward field-aligned current equatorward of the westward electrojet is called the Region 2 field-aligned current, the other upward field-aligned current has many names partly because it changes dynamically. We discuss the current system further in section 4.2.

The morning activity expanded westward toward midnight along about 70 degrees, while the evening-midnight activity expanded poleward from 65 degrees toward higher latitudes. As the result of expansion, these two regions of the westward electrojets merged at the midnight high-latitude sector in the spatial resolution of the existing ground stations. The timing of this merging (06:16-06:17 UT) coincides with the onset of a sharp change of ΔBx at the IQA station (291 long = 0130 LT = 02 MLT, 74 GMLat) with ΔBx < -3000 nT at 06:17-06:18 UT. This is the largest ΔBx during the first 20 minutes although only a small positive deviation was registered between 06:11-

06:16 UT at this station. When IQA was experiencing this sharp development, the evening-midnight activity in the auroral region at < 69 GMLat already started to decay, making the IQA station a single point of outstanding high activity. IQA is located on the same meridian as GOES-12 during this period (cf. Figure 4), and GOES-12 detected an unusual sharp change in the magnetic field as described in the next subsection.

3.2. GEOSYNCHRONOUS SATELLITE DATA

As shown in the previous subsection, the ground-based magnetometers detected the onset of the 2000 nT level westward electrojet at 06:12 UT in one-minute resolution in both hemispheres. At the same time, the geosynchronous satellite in the midnight sector detected the substorm signature. Both GOES-10 and GOES-12 detected the arrival of the shock at around 06:11:40 UT as a faint decrease in elevation angle (inc = atan(H_P/H_E)), which means a stretching of the geomagnetic field. This is immediately followed by a recovery of elevation angle starting at around 06:12:00 UT in both the GOES-12 (01 LT) and GOES-10 (21 LT) data as shown in Figure 4. Recovery of the elevation angle is normally used as the signature of a dipolarization [H. Singer, privation communication, 2005].

Accordingly, the polar angle (dip = acos($H_P/|B|$)) in the GOES-12 data also increased after the shock arrival and decreased after 06:12:00 UT. However, the behaviors of the elevation angle and the polar angle are quite different in the GOES-10 data. This is because the cross-tail current sheet passed through the satellite at 06:12:10 UT and 06:13:20 UT as is seen from the sign of the Earthward field. In fact the elevation angle behaved quite differently between GOES-10 and GOES-12. In this case, one cannot really discuss the dipolarization or the plasma sheet thinning from the elevation angle only.

Fortunately, one can estimate the variation of the total cross-tail current near GOES-10 because GOES-10 and Polar were located within 1 R_E distance of each other during this period. The difference in the magnetic field between these two spacecraft roughly gives the total electric current between the spacecraft according to the Ampere's law [Iijima and Potemra, 1976]. Both satellites are located east of CMO station and west of the other stations (cf. Figure 7b) that detected the ground onset of the evening-midnight activity at 06:12 UT.

Let us concentrate on the initial two minutes after the shock arrival. Note that the value during the short gap in the plot of Polar data (06:11:40 - 06:12:20 UT) is rather smooth (without extra peaks) in the unqualified plot (not plotted here), and we do not lose so much information during this 40 sec. The difference in the eastward fields between the satellites showed a large variation, from +20 nT (we take Polar minus GOES-10) at the shock arrival (06:11:40 UT) to -30 nT at 06:12:20 UT, -60 nT at 06:13:00 UT, and -10 nT at 06:14:00 UT. The difference in the Earthward fields between the satellites also

showed a large variation, from +70 nT at the shock arrival to +150 nT when the current sheet moved the north of GOES-10 at 06:12:20 UT, +100 nT at 06:13.00 UT, and +80 nT at 06:14:00 UT. The difference in the poleward fields between the satellites showed the smallest variation, i.e., -10 ~ -20 nT all the time from the shock arrival.

As a total, the Polar magnetic field became more sun-pointing than the GOES-10 magnetic field during the first minute after the shock arrival, and this difference is roughly maintained afterward. Since Polar was located north of GOES-10, this immediately means an increase of duskward cross-tail current between the spacecraft. The observed increase of the current is caused either by the actual increase of the current intensity or by the north-south motion of the existing non-uniform current sheet. In the former case, the magnetic field at 21 LT was more tail-like at 06:12:20 UT than at the shock arrival.

No matter which is the case, we cannot conclude any dipolarization between 06:11:40 UT and 06:12:20 UT although the elevation angle drastically increased at GOES-10. This result agrees with the electric field data of the Polar satellite although only the component in the spin plane is measured (not shown here). The electric field shows a short bump of 20 mV/m at around 06:12:15 ~ 06:12:30 UT but nearly zero before 06:12:15 UT except the Z (poleward) component that started to deviate at 06:12:00 UT.

The largest decrease of the current between the two spacecraft is observed between 06:13:00 and 06:14:00 UT. Correspondingly, a large deviation of the electric field started from 06:13:00 UT toward the peak of 40~50 mV/m at around 06:14:00 UT. This indicates a disruption of the current by the anomalous resistively at 21 LT.

Later at 06:16:40 UT, GOES-12 registered a sharp increase of all components (H_N, H_P, and H_E) with a short preceding spiky decrease. This is the same timing as the beginning of the ΔBx = -4000 nT geomagnetic deviation at the IQA station, which is located at the same meridian as GOES-12. GOES-10 did not observe this signature (it instead detected a short positive spike 30 sec later). The sharp decrease of ground geomagnetic field (horizontal component) is also a local phenomenon as described in section 3.1. Both the ground and the satellite data indicate that this is a local independent onset of a new activity and is not a simple extension of previous activities.

Let us also examine the morning activity. In Figure 3, the LANL-01A satellite located at 07 LT detected several spikes during the first several minutes after the shock arrival at 06:11:10 UT. If these multiple spikes are caused by the passage of the shock, we should also detect a passage of magnetic vortex at ground, but this was not the case. Therefore, these multiple spikes are most likely associated with the large ΔBx (or westward electrojet) in the morning stations. On the other hand, this is less likely related to the cusp where we sometimes observe energetic particles [Kremser et al., 1995]. Although the strong IMF B_Y moves the cusp in either morning side or afternoon

side at high-latitude and its conjugate region, this effect is anti-symmetric, i.e., a dawnward IMF B_Y moves the northern cusp prenoon and southern cusp postnoon. That makes the equatorial region dawn-dusk symmetric. However, LANL detect the multiple-peaks only at prenoon (LANL-01A) but not postnoon (LANL-02A). Thus the LANL data indicates an exclusive morning activity. It is possible that a locally-closed current system between the ionosphere and the plasma sheet in the morning sector caused both the ground ΔBx and multiple spikes at the LANL-01A satellite.

3.3. IMAGE FUV DATA

%%%%%% Figure 8 %%%%%%

Figure 8 shows a sequence of IMAGE-FUV [Mende et al., 2000] over the southern hemisphere during the initial phase of this magnetic storm. At 06:11:40 UT (Figure 8a), only the residual from the previous auroral arc (an oval in the entire morning and a bright region in the midnight sector from which a polar arc extends) was recognized. At 06:13:40 UT (Figure 8b), the midnight spot and the morning arc were suddenly intensified. The former timing corresponds to the time when the shock is passing through the magnetosphere, and the latter timing corresponds to the beginning of the large negative ΔBx registered at both the morning and the evening geomagnetic stations.

In the next two images at 06:15:40 UT (Figure 8c) and 06:17:40 UT (Figure 8d), one can recognize expansions of the brightened area of both the morning arc westward (toward midnight) and the midnight spot poleward (not westward at all). The morphologies of the expansion are different between these two bright areas, making the contrast between the morning broad arc and the midnight round spot clearer. If looking at a fixed location, the activity at the local midnight is decaying whereas the morning activity is sustained during two images. Thus the midnight spot and the morning arc independently broadened and brightened each other, and hence we can conclude that these simultaneous activities are independent of each other. This is what we have already concluded from the ground geomagnetic field data.

The independent auroral activities, one in the morning sector and the other in the midnight sector, merged with each other at 06:17:40 UT, making the auroral form similar to an ordinary substorm in the next image (06:19:50 UT, not shown here). When the merging took place at 06:17:40 UT, a very bright spot appeared in the merging region at 03 MLT in Figure 8d. On the other hand, the third geomagnetic activity (4000 nT deviation) that started at 06:17 UT is very localized at around 01 LT (or 02 MLT, the IQA station only) in the northern hemisphere. A similar offset is found in the first activity in the midnight sector. Before the merging, the midnight auroral activity in the southern hemisphere is centered at post-midnight (Figure 8) whereas the

midnight geomagnetic activity in the northern hemisphere is centered at pre-midnight in both geographic and geomagnetic coordinate.

As mentioned in section 3.1, the ground geomagnetic deviation shows the inter-hemispheric difference, and this is most likely due to the large dipole tilt (22~23 degree during this short period). This fact makes it difficult to simply map the southern hemispheric auroral image to the northern hemisphere. The finite IMF B_Y also distorts the inter-hemispheric mapping relation in the azimuthal (local time) direction. Together with the ambiguity in estimating the local time from the obliquely taken images, the inter-hemispheric difference of location could be as large as a few hours in local time.

Here, we estimate it from the location of the third activity as 1~2 hours in local time. This is a reasonable correction if one compares the auroral activity in the midnight sector (Figure 8) and the geomagnetic disturbances in the pre-midnight sector (Figure 7). Note that the corresponding local time on the equatorial plane is similar to that of the northern hemisphere because the equatorial plane is much closer to the northern polar region than the southern polar region due the 22~23 degree dipole tilt.

To examine the rational of this correction, we made a field-line tracing using Tsyganenko-96 geomagnetic field model [Tsyganenko, 1995; Tsyganenko and Stern, 1996] and Geopack-3 mapping code [Tsyganenko, 2003]. We calculated the foot points of GEOS-12 for three cases: (P_D (nP), Dst (nT), IMF B_Y (nT), IMF B_Z (nT)) = (0.1, 0, 0, 0), (10, -50, -5, -3), and (80, +50, -20, -20), where P_D is the solar wind dynamic pressure. The second case roughly corresponds to the condition before the SC, and the third case to that after the start of SC. While the foot longitude in the northern hemisphere stays the same (279~280 long or 01 MLT) for all three cases, the foot longitude in the southern hemisphere drastically changes, from about 240 long (01 MLT) for the first (quiet) case, to about 270 long (0130 MLT) for the second case, and to about 305 long (0230 MLT) for the third case.

Note that the solar wind condition during this period is outside the range of data set from which existing magnetic field models are derived, and hence one may not make a quantitative argument using existing magnetic field model particularly for dayside. Yet we have a good agreement in the inter-hemispheric longitudinal shift between the observation and the model. Therefore, we can safely conclude that the IQA station and GOES-12 are on the same local time sector whereas the corresponding local time in the southern hemisphere shifts eastward by 1~2 hours in MLT.

With this inter-hemispheric correction in the local time in mind, one may compare the common large-scale feature in the northern hemisphere (geomagnetic field data) and southern hemisphere (optical data). Both the optical data by IMAGE/FUV and the ground-based magnetometer data show that the timing (06:17 UT) and location (02 MLT in the northern hemisphere) of the onset of the huge and rapid activity (3000 nT in

2min) match with those of a spike-like signature at the GOES-12 satellite at 06:16:40 UT as well as with those of the merging of the evening auroral activity and the morning auroral activity in the opposite hemisphere. This coincidence suggests that the extremely rapid development toward ΔBx = -4000 nT at the IQA station, only 6 minutes after the start of SC, might not be a simple extension of the midnight activity, but a result of the merging of two independent 2000 nT level activities. Then the question is if this is true or not, and what is the mechanism if it is true. We have no concrete answer to this question but discuss it later in section 4.3.

In summary, the IMAGE-FUV data support the scenario derived from the ground-based magnetometer data although it is inconclusive: (1) Two strong ionospheric electric current systems with westward electrojets (both with a level of 2000 nT) started independently and simultaneously in the morning sector and the evening-midnight sector immediately after the SC was recognized. (2) An extremely large activity (level of 4000 nT) started when and where the above two activities met in the post-midnight sector.

3.4. SUMMARY OF THE INITIAL 10 MINUTES

Table 1 summarizes the time sequence from the shock arrival to the onsets of the largest geomagnetic activity at the IQA station. Each column lists the activities in the magnetosphere, the ground geomagnetic field, and the aurora, respectively. The onset of the large expansive activity in the evening-midnight sector was at 06:12 UT, while the onset of the strong ionospheric current system similar to those of substorms was recognized in the morning sector at either 06:12 UT or 06:13 UT (cannot be distinguished from the SC signature). The onset of the localized 4000 nT activity at the high-latitude post-midnight (02 MLT) region was at 06:16-06:17 UT. Corresponding activities are found in the southern hemisphere. The inter-hemispheric offset of the local time during this period is 1~2 hours, i.e., 02 MLT in the northern hemisphere corresponds to 03~04 MLT in the southern hemisphere and to the local time sector of GOES-12.

%%%%%% Table 1 %%%%%%

The morphology (expansion of both the westward electrojet and aurora), the activity level (2000 nT magnetic deviation and the brightness of aurora), and the dynamic change of the cross-tail current make both the evening-midnight activity and the morning activity fall into the category of strong substorm expansion in the classic definition. On the other hand, the substorm is a global phenomenon in the classic definition too. The pseudo-breakup [e.g., Koskinen et al., 1992; and references therein] is the only category that the present activities may fall into, but no pseudo-breakup as strong as 2000 nT has ever been observed. We rather consider that each activity could

have expanded globally if these two activities did not merge. In this sense we can call these activities substorms, although they are not standard ones.

4. DISCUSSION

During the initial 6 minutes after the SC was recognized at 06:11:21 UT, three onsets of large geomagnetic activities of AL<-2000 nT associated with strong westward electrojets were observed together with auroral brightening. The first two activities, one in the midnight sector starting at 06:12 UT, and the other in the morning sector starting at 06:12~06:13 UT, have the characteristics of substorm expansion, although they are independent of each other and their expansions are limited to the respective local regions during this 6 minutes. The third activity is a sharp drop of ΔBx only at the IQA station (02 MLT) reaching about -4000 nT together with a spike-like change of the magnetic field at GOES-12 on the same meridian 5 minutes after the other onsets. This localized activity corresponds to intense aurora localized at 03 MLT in the southern hemisphere. All these facts as well as their intensity make the initial phase of this magnetic storm unique. The immediate question is the nature and the triggering mechanism of these three activities.

4.1. TRIGGERING AND ENERGY SUPPLY

The perfect match in timing between the SC and the substorm onsets in both the midnight and the morning sectors indicates that these particular substorms are triggered by the shock arrival. In fact the pressure pulse of the solar wind is known to trigger some substorms directly (by anonymous mechanisms, e.g., current sheet instability or direct disruption of current by electric field or waves or pressure, etc.) or indirectly (through, e.g., tail reconnection) [e.g., Lui et al., 2005; Lyons et al., 2003; Meurant et al., 2003; Zhou et al., 2003; and references therein]. If the triggering of the present substorms were independent of the shock arrival, this triggering should have taken place within a short window (less than one minute) such that the dipolarization at GOES satellites should not take place before the shock arrival. Such a pure coincidental chance is less than one percent (a less than one-minute window divided by the average interval time between two onsets (which is > 2 hour [Borovsky et al., 1993])). Therefore, the onset of the observed activities at 0612 UT is most likely (>99 % probability) triggered by the arrival of the shock, and we do not consider the unlike possibility of coincidence.

All the widely-accepted substorm models predict the substorm onset location in the near-Earth plasma sheet ranging from several R_E to 30 R_E depending on which model [e.g., Ohtani, 2004; Lyons and Wang, 2004; Lui et al., 2005, and references therein]. Reconnection models predict the onset location outside the geosynchronous orbit, and non-reconnection models predict it inside 10 R_E. Since the shock propagation velocity

is consistently high at 0.3 R_E/sec throughout the interplanetary space and magnetosphere as summarized in Figure 6, the shock could not have arrived at the tail earlier than it is detected at GOES and Polar by traveling through the magnetosheath instead of the magnetosphere.

Now we examine the time sequence. The ground-based magnetometer data shows that the onset of the substorm expansive phase in the evening-midnight sector is 06:12 UT in one-minute resolution in the both hemispheres whereas the GOES and Polar satellites indicate that the depolarization is after 06:12:20 UT in 5-seconds resolution (the elevation angle of the magnetic field increased drastically at GOES-10 after 06:12:00 UT, though). Considering the Alfvén transit time between the geosynchronous location and the ground (which is about 1~3 minutes), the dipolarization timing at the GOES location is too late to cause the onset on the ground (Alfvén velocity is slower than the shock propagation velocity). On the other hand, the shock arrival at the nightside inner magnetosphere is between 06:11:20 UT and 06:11:30 UT, and hence the triggering is not before 06:11:20 and not after 06:12:00 UT. Therefore, the magnetospheric onset site of the substorm expansive phase must be between the Earth and the GOES satellites. This location is not favorable to the reconnection models, in which the near-Earth onset is caused by the sunward flow that is driven by the reconnection > 6 R_E. The shock arrival at the reconnection site cannot be before 06:11:30 UT as mentioned above, and it is impossible to progress from the Earthward plasma acceleration at > 6 R_E to the transmission of sufficient electric field (which should be carried by the Alfvén velocity) into the ionosphere within one minute. In fact Polar electric field data did not detect any signature of such Earthward convection until 06:12:15 UT.

The triggering problem is related to the energy feeding problem after the onset. For several hours before the SC, IMF B_Z was about 0 ~ -5 nT, AL was 200~300 nT (not really quiet), and some plasma sheet thinning was recognized by the GOES satellites. ACE registered a short period (9 minutes) of large negative B_Z (~ -8 nT) at about 13 minutes before the shock, while this period of B_Z ~ -8 nT is reduced to only 3 minutes at Geotail. From this background, the energy stored in the magnetotail before the SC may be enough to cause an ordinary substorm. However, the observed IMF condition (with small B_Z during the last hour) normally does not cause an extremely large westward electrojet with AL~-2000 nT. We are not aware of any report showing AL<-2000 nT activity without a long (>15 min) period of southward IMF (B_Z<-5nT). We looked through uncalibrated AE during 2002, 2003, 2004, and first half of 2005, and found only 11 days with activity of AL<-2000 nT (one, three, four, and three days in 2002, 2003, 2004, 2005, respectively). All except two events (the January 21, 2005 event and this event) are preceded by long (>15 min) periods of southward IMF (B_Z<-5nT). Thus, the IMF condition before the SC is not favorable for storing sufficient magnetic energy in the magnetosphere to cause the observed westward electrojet AL<-2000 nT by just releasing the energy.

Yet we observed a sharp decrease of AL reaching AL<-2000 nT within 5 minutes after the shock arrival. Furthermore, the GOES and Polar data indicate that the cross-tail current did not substantially decrease after the onset. It decreased briefly during 06:13:00-06:14:20 UT, but the thin plasma sheet recovered afterward. Thus the stored magnetic energy did not decrease after the onset at the geosynchronous orbit. From these facts, the majority of the substorm energy until the merging of the two activities at 06:16 UT is most likely powered directly from the solar wind (i.e., solar wind-magnetosphere dynamo) rather than released from the stored energy in the magnetosphere. This means that if tail reconnection is ever responsible for such a sustained energy conversion, the configuration of the near-Earth x-point must be stationary with a narrow exit angle. The problem of the mechanisms of the triggering and the energy feeding requires lengthy dedicated discussion, which is beyond the scope of this paper.

4.2. NATURE OF MORNING ACTIVITY

The largest question on the morning activity concerns the similarity to and difference from ordinary substorms. The morning activity has a classic signature of a substorm: the sudden intensification of both the aurora and the westward ionospheric Hall current, and the subsequent westward expansion of both the aurora and the electrojet.

On the other hand, a solar wind pressure pulse is known to intensify the dayside auroral activity as a part of the dayside magnetospheric boundary phenomena [Sandholt et al., 1994]. The majority of the global auroral brightenings in response to the interplanetary shock on the dayside do not accompany large development of the westward electrojet. Therefore, auroral brightenings in the morning and afternoon sectors immediately after the start of SC are often interpreted as the signature of SC-related non-substorm activity rather than substorm-related activity [Zesta el et al., 2000; Chua et al., 2001; Zhou et al., 2003]. SC-related activity includes the Kelvin-Helmholtz-type vortex and the cusp-related aurora [Elphinstone et al., 1993; Sandholt et al., 1994; Zhou et al., 2003]. The locations of these activities are mapped to the magnetopause or the plasma mantle. Another type of SC-related activity is a stimulation of field-aligned current by the Alfvén wave [Chua et al., 2001; Zhou et al., 2003]. In both cases of SC-related activities, the brightening of the aurora takes place first at noon, then rapidly expands from noon to midnight through both the morning and the afternoon sides of the auroral oval.

However, the observation shows a steady increase of the westward electrojet and its expansion rather than propagation, as described in section 3.1. The extremely high intensity (deviation < -2000 nT) corresponding to sunward convection also indicates that there is a strong dynamo in the sunward convection region inside the magnetosphere. These features resemble those of substorm expansion rather than those of the SC-related boundary process.

Before concluding so, let us examine the mapping relation as illustrated in Figure 9. If the observed activity in the morning sector is mapped to the magnetospheric boundary, then the direct solar wind interaction (direct inflowing into the magnetosphere) could be the source of the aurora and ionospheric electric field in spite of the substorm-like morphology. If the observed activity is mapped to the inner magnetosphere such as the plasma sheet, then we cannot distinguish this activity from a substorm, although the region is limited to the morning side. The key information is then the location of the polar cap boundary.

%%%%%% Figure 9 %%%%%%

The observed activity can also be mapped to both the magnetospheric boundary and the inner magnetosphere. For example, the eastward electrojet (anti-sunward convection) inside the polar cap at 07 LT (the BJN station) is as strong as the westward electrojet (sunward convection) at lower latitudes on the same meridian (TRO and ABK) until 06:16 UT, although the westward electrojet at the kernel of the morning activity (LRV, 04 LT) is much stronger than the eastward electrojet in the polar cap (GDH, HRN, or BJN) or the westward electrojet in the late morning sector (TRO or ABK). Therefore, the mapping relations could be different between from 07 LT and from 04 LT. To avoid the confusion we examine the kernel of the activity, i.e., at the LRV station at 04 LT.

The best clue is direct detection of the polar cap boundary. Low-altitude satellites can provide a snapshot of locations of key regions such as the polar cap, boundary layer, and the plasma sheet. Unfortunately, none of the FAST and DMSP satellites, those which are capable of identifying the region, traversed the dayside polar region during 06:10-06:20 UT. The closest dayside traversals were after 06:35 UT by DMSP-F13 from early afternoon to late morning and before 06:05 UT by DMSP-F15 from afternoon to noon, both in the northern hemisphere. When DMSP-F13 passed the convection reversal in the morning sector at 06:51 UT, the morning geomagnetic stations had just finished the period of negative ΔBx. Another clue to detect the polar cap boundary and the cusp is the 2-D ionospheric convection pattern observed by HF radars because the 2-D ionospheric convection directly reflects the instantaneous location of the polar cap boundary. However, the Cutlass HF radar, which covers the prenoon polar region at 6-7 UT, detected very weak signals because of the very disturbed ionospheric conditions after this strong SC, and it cannot give the convection data [M. Lester, private communication, 2005].

Since no observation is available in determining the polar cap boundary, we have to rely on a magnetic field model, although it can be used only for qualitative argument as mentioned in section 3.3. We again made a field-line tracing using the Tsyganenko-96 model for different sets of parameters: (P_D (nP), Dst (nT), IMF B_Y (nT), IMF B_Z (nT)) =

(0.1, 0, 0, 0), (10, -50, -5, -3), (30, -50, ±10, -10), (50, -50, ±15, -15), and (80, ±50, ±20, -20). The IMF observed by Geotail and ACE is strongly dawnward before the SC (about -5 nT entire hour) and during the SC (fluctuating but rather $B_Y<0$ than $B_Y>0$ during the first several minutes). Unless the IMF is strongly duskward ($B_Y < +10$nT), the LRV station is mapped to the same magnetic latitude (-69 GMLat) and several degrees equatorward of the polar cap with different longitude (more eastward for larger $B_Y>0$). In general the IMF B_Y effect does not drastically change the mapping relation at this latitude.

The latitude of the auroral arc seen by IMAGE (65 GMLat south) is nearly the same as the latitude of Region 2 upward field-aligned current in the other (northern) hemisphere obtained from the ground-based magnetometer data, and is 3~4 degree equatorward of the convection reversal or Region 1 downward field-aligned current. This indicates both the aurora in the southern hemisphere and the westward electrojet in the northern hemisphere are connected to the inner magnetosphere but not the magnetospheric boundary layer.

Furthermore, the westward electrojet is observed at higher latitude at 04 LT (LRV) than at 07 LT (TRO) whereas the auroral arc is observed at lower latitude at 04-05 LT than at 07-08 LT. Even if the auroral arc in the southern hemisphere might correspond to the convection reversal and to the magnetospheric boundary region at 07 LT, the aurora at 04~05 MLT in the southern hemisphere is most likely mapped to Region 2 field-aligned current rather than Region 1 field-aligned current at 03~04 LT in the northern hemisphere. With this mapping relation, the morning activity satisfies the classic definition of a substorm.

The auroral arc seen in the IMAGE data is very narrow indicating discrete aurorae, and such discrete aurorae normally correspond to upward field-aligned currents with some exceptions [Morooka et al., 1998]. Inversely, a strong upward current means electron precipitation accelerated by parallel electric field according to the Knight's law [Knight, 1973], and hence it normally causes a discrete aurora. Taking into consideration the latitudinal coincidence, the intense aurora in the southern hemisphere most likely corresponds to the Region 2 upward field-aligned current in the northern hemisphere equatorward of the westward electrojet, although the exact conjugacy is not required for the present discussion (discrete auroral forms are often non-conjugate [e.g. Stenbaek-Nelson and Otto, 1997]).

One may yet argue that the present event is unusual and general rules might not apply because what we need to know is the actual magnetospheric configuration which is determined by the long history of IMF [Cumnock et al., 1997]. For example if the magnetospheric condition corresponds to a strongly duskward IMF, the LRV station can be mapped to the polar cap. According to the Tsyganenko-96 model, a condition with B_Y=+15nT and B_Z=-15nT makes such a mapping relation.

A faint auroral arc is recognized poleward of the ordinary arc in the dawn sector in Figure 8a. The observed location of the transpolar arc indicates that the magnetospheric morphology (i.e., mapping relation) might reflect a weakly IMF $B_Y>0$ condition [Craven et al., 1991; Elphinstone et al., 1993] despite the measured $B_Y<0$ condition for the entire hour before the SC. However it is difficult to assume a strong duskward B_Y (>+10nT) effect just from this. Note that the mapping relation at midnight well agree with a dawnward IMF as discussed in section 3.3, and duskward IMF condition is limited to dayside or polar cap in this case. A moderately duskward IMF (B_Y=+10nT with B_Z=-10nT) makes the LRV station well equatorward of the polar cap boundary. Therefore, both the observed strong westward electrojet and aurora are located far equatorward of pole cap boundary in these cases.

Thus, the possible IMF B_Y effect should not alter our conclusion: the intensification and expansion of the aurora and the westward electrojet in the early morning sector took place well equatorward of polar cap boundary, and hence they are connected to the inner magnetosphere but not to the magnetospheric boundary. Together with the expanding features of strong geomagnetic and auroral activities, the morning activity, which is independent of the evening-midnight expansion, has all the classic characteristics of substorm expansion. In other words we have simultaneous substorm onsets of the classic definition at two different locations, one somewhere between 21-01 LT (from CMO to PBQ), and the other near the LRV station (04 LT).

Simultaneous brightening of global auroral arcs in response to the pressure pulse has recently been reported in the different context of substorms [Chua et al., 2001; Boudouridis et al., 2003; Meurant et al. 2003]. However, these global auroral brightening events do not accompany very strong westward electrojets (mostly < 500 nT in the morning sector), and in this sense the present event is different. One may not dismiss an geomagnetic activity of > 2000 nT with classic features of substorm onset from a substorm.

4.3. ONSET OF 4000 nT ACTIVITY

A local but extremely large geomagnetic activity (~4000 nT) started at 06:17 UT at 02 MLT (the IQA station). This location and timing match those of the merging of the morning aurora and the midnight aurora, which were both expanding. They also match those of a sharp change in the magnetic field with a short spike at the geosynchronous satellites (only GOES-12 but not GOES-10) at 06:17:40 UT. These coincidences indicate that these phenomena (merging and onsets) are related; i.e., the last activity might be triggered by the merging of two preceding substorms.

The detail of this onset and its exact mechanism are unknown due to the lack of observation points at this local time and latitude. Here, we just point out one

possibility: namely, an instantaneous approach of the convection reversal in the morning sector (which is connected to the magnetospheric boundary) to the midnight activity from the polar cap side. This possibility has never been considered in the past, but it is not impossible if the magnetopause surface wave becomes extremely large while the magnetopause shrinks due to the extremely high solar wind dynamic pressure (the highest solar wind velocity in history) and the fluctuating strong IMF. In fact the short-lived spike in the GOES-12 data means that a very quick change of the contributing current sheet happened at around 06:17 UT at this particular local time. Furthermore, a signature of shrinked near-tail magnetopause is observed at the shock arrival.

In Figure 4, total magnetic fields (|B|) observed by GOES-12 (01 LT) and Polar (21 LT, or X_{GSM} = -5.3 R_E, Y_{GSM} = +4.8 R_E, Z_{GSM} = -0.7 R_E) increased at the shock arrival while |B| decreased at GOES-10 (21 LT, or X_{GSM} = -5.1 R_E, Y_{GSM} = +4.0 R_E, Z_{GSM} = -1.5 R_E). The discrepancy between Polar and GOES-10, which are located close to each other (~1 R_E), is difficult to understand unless we assume completely different influences of the magnetopause current and the cross-tail current between these two satellite locations. Inversely such a local difference between Polar and GOES-10 can be understood if the magnetopause is located relatively close to these spacecraft. Such an enhanced contribution from the magnetopause current is eventually predicted during the extremely high solar wind dynamic pressure conditions according to the Tyganenko-01 model [C.T. Russell, private communication, 2005].

Thus it is possible that the extremely high solar wind dynamic pressure pressed the magnetopause very close to the central plasma sheet. Furthermore, the magnetopause must be very wavy in response to the shock arrival, and in fact a large amplitude Pc-5 is observed at the ground as mentioned in section 3.1. With this background, the topside magnetopause may have partially flashed through the nightside magnetosphere at around 06:17 UT. If the enhanced magnetopause current approaches the plasma sheet, the oppositely-directed sheet currents during this short period may produce the spike-like change in the geomagnetic field at GOES-12. If this is the case, we may state that the last activity starting from 06:17 UT at around 02~03 MLT is triggered by the meeting of two activities, one in the evening-midnight sector, and the other in the morning sector.

Unfortunately we cannot examine this scenario because of the lack of sufficient data/stations. To test this idea, we need at least three times more ground stations in the longitudinal direction. Such tests would be quite difficult even in the near future because the solar wind velocity of 2000 km/s does not occur very often. However, we have one possibility. If this scenario is correct, we can expect similar phenomena in the other magnetized planets which are subject to strong solar wind effects compared to their magnetospheric size. Mercury is one such planet, and one can examine this

scenario in the future Mercury magnetospheric missions such as Bepi-Colombo [e.g., ESA web site, http://www.esa.int/esaSC/120391_index_0_m.html].

5. SUMMARY AND CONCLUSIONS

Multiple data sets from ground-based magnetometers, satellite auroral images, and in-situ data from geosynchronous satellites show several unusual features of the geomagnetic activities during the initial phase of the magnetic storm starting at 06:11 UT on October, 29. 2003. Three different strong westward electrojets of > 2000 nT level are observed during the initial 10 minutes after the start of SC. SYM-H was positive during this period, i.e., the period is during the initial (compression) phase of the magnetic storm. The first two activities satisfy the classic definition of substorm expansions and started independently of each other immediately after the SC was recognized in the evening-midnight sector and the morning sector, respectively. Considering its intensity and quickness, we should call them substorm expansions although the double onset locations make them non-standard. The last activity started when and where the previous two activities met at around 02 MLT (in the northern hemisphere, and 03 MLT in the southern hemisphere) 6 minutes after the start of SC. The IMF condition before the SC had not been favorable in causing a strong substorm activity with $\Delta B < -2000$ nT.

Such a quick development of extremely strong activity (> 2000 nT geomagnetic deviation within 5 minutes from the start of SC) has never been reported previously. Two simultaneous but independent onsets of substorm expansions in the classic definition, although their activities are limited to either midnight sector or morning sector, are another unusual feature of this event. Finally the quick development (3000 nT in 2 minutes) of local activity (IQA station only) together with spike-like signature at GOES-12 is the other unusual feature. Since the initial 10 minutes of the magnetic storm is thus unique, we described each event using as large body of data as possible.

The minute-to-minute observations are given in Table 1. They are summarized as follows:
(1) The arrival of the interplanetary shock swept the magnetosphere quickly from the dayside to nightside with a velocity similar to the interplanetary shock velocity (about 0.3 R_E/sec). The consistent propagation velocity throughout the upstream interplanetary space, the magnetosphere, and the downstream interplanetary space allows us to estimate the arrival time of the shock in 10-seconds accuracy in the near-Earth tail where no satellite was located.
(2) In 1-second resolution data, the SC appeared on the ground nearly simultaneously at both dayside mid-latitude stations and a morning high-latitude station (KRN) at 06:11:21 UT.

(3) The evening-midnight activity starting 06:12 UT, i.e., right after the SC was recognized showed quick development of a strong westward electrojet (reaching $\Delta B<-1000$ nT at 06:13 UT, and $\Delta B<2000$ nT at 06:16 UT) and intense aurora, both expanding poleward. These characteristics are typical ones of substorm expansion.
(4) The morning activity starting either 06:12 UT or 06:13 UT, i.e., right after the start of SC also showed a quick development of a strong westward electrojet (reaching $\Delta B<2000$ nT at 06:15 UT) and intense aurora, both steadily expanding in the azimuthal direction at around 65 GMLat. The activity also accompanies an eastward electrojet at poleward stations (> 70 GMLat). This activity, at least for its kernel at 04 LT (05~06 MLT) in the northern hemisphere, is not mapped to the magnetospheric boundary, but rather to the plasma sheet. These characteristics are again typical ones of substorm expansion.
(5) The onset time of the current sheet activity at the geosynchronous satellites are 06:12:00 UT (only a half minute after the shock arrival), but substantial current disruption and electric field enhancement did not start until 06:13:00 UT.
(6) The last activity started at 06:17 UT at post-midnight when two activities met at high-latitude midnight 6 minutes after onset, and registered a 3000 nT change within 2 minutes (maximum of nearly 4000 nT at 10 minutes after the start of SC). The GOES-12 magnetic field at the same meridian showed a local (seen only in GOES-12) spiky increase in all components of the magnetic field at this onset time (06:16:40 UT).

The first substorm onset in the evening-midnight sector started less than one minute after the shock arrival at near-Earth tail. From the timing, this activity is most likely directly triggered by the shock arrival. Similarly the second substorm onset in the morning sector is most likely triggered by the shock arrival. A further examination of the shock arrival timing and onset timing at ground and the geosynchronous satellites leads us to conclude that the magnetospheric onset location is inside the geosynchronous orbit. From these facts, this particular onset is less likely triggered by magnetotail reconnection. Considering the IMF condition before the SC, the observed 2000 nT activity is most likely maintained by the energy pumping from the solar wind (i.e., solar wind-magnetosphere dynamo) rather than the release of the stored energy although we cannot answer how this dynamo was formed.

The last activity is difficult to understand partly because of its extremely high activity (3000 nT change in 2 minutes) at one local station (IQA) only and partly because of the unusual behavior of the associated spiky enhancement of the magnetic field observed by GOES-12. We proposed a new scenario in which a part of the dayside field-aligned current system is detached and swept tailward, briefly passing very close to the substorm current system, and that this passage triggered the third activity.

ACKNOWLEDGEMENT

We thank H. Singer, T. Nagai, and C.T. Russell for useful comments for understanding the GOES, Geotail and Polar data that they provided, respectively. Thanks are also to Mark Lester at Leicester University for providing and interpreting Cutlass HF data, to T. Horbury at Imperial College for identifying the shock arrival timing detected by Cluster magnetic field data, to T. Kamei at WDC-C2, Kyoto University for calculating the AE index, and to S. Akasofu for useful comments. We also thank the following organizations and teams for providing the data presented here.

Geomagnetic field data is provided by British Geological Survey (BGS), Danish Meteorological Institute (DMI), Ecole et Observatoire des Sciences de la Terre (EOST), Finnish Meteorological Institute (FMI), Finnish Academy of Science, Geological Survey of Canada (GSC), Geological Survey of Sweden, Geoscience Australia, Institute of Geological and Nuclear Sciences, Institute of Solar-Terrestrial Physics (ISTP) at Irkutsk, The Irish Meteorological Service, Leirvogur geomagnetic station, Lviv Centre of Institute of Space Research, National Institute of Information and Communications Technology (NICT), Polish Academy of Sciences, Tromsoe Geophysical Observatory in Norway, and United States Geological Survey (USGS), partly through INTERMAGNET.

ACE magnetic field data is provided by the ACE/MAG team (PI: N. Ness at Bartol Research Institute) and the ACE Science Center. Geotail magnetic field data is provided by Geotail/MGF team (PI: T. Nagai at Tokyo Institute of Technology) and the ISAS/Geotail project. WIND magnetic field data is provided by WIND/MFI team (PI: R. Lepping at NASA/GSFC) and NASA/WIND project. POLAR magnetic field data is provided by POLAR/MFE team (PI: C.T. Russell at IGPP) and NASA/POLAR project. POLAR electric field data is provided by POLAR/EFI team (PI: F. Mozer at UCB/SSL) and NASA/POLAR project. Cluster magnetic field data is provided by Cluster/FGM team (PI: A. Balogh at Imperial College) and ESA/Cluster project. GOES magnetic field data is provided by GOES magnetic field team (PI: H. Singer at NOAA) and NOAA/GOES project, and prepared by A. Newman. LANL satellite project is managed by Los-Alamos National Laboratory, and IMAGE project is supported by NASA. The Cluster and Polar particle data for shock identification are provided by Cluster CIS team (PI: H. Reme at CESR) and Polar HYDRO team (PI: J. Scudder at Univ. Iowa) through NASA CDAweb (http://cdaweb.gsfc.nasa.gov/). DMSP convection data is provided by Center for Space Sciences at the University of Texas at Dallas and the US Air Force.

MY thanks programs for disabled people in Sweden which have made it possible for him to work.

REFERENCES

Akasofu, S.-I. (1964), The development of the auroral substorm, *Planet. Space Sci., 12*, 273.

Akasofu, S.-I. (2004), Several 'Controversial' Issues on Substorms, *Space Sci. Rev., 113*, 1-40, doi: 10.1023/B:SPAC.0000042938.57710.fb.

Akasofu, S.-I. and S. Chapman (1972), *Solar-Terrestrial Physics*, Oxford Clarendon Press.

Araki, T., S. Fujitani, M. Emoto, K. Yumoto, et al. (1997), Anomalous sudden commencement on March 24, 1991, *J. Geophys. Res., 102*(A7), 14075-14086.

Asano, Y., T. Mukai, M. Hoshino, Y. Saito, H. Hayakawa, and T. Nagai (2004), Statistical study of thin current sheet evolution around substorm onset, *J. Geophys. Res., 109*, A05213, doi:10.1029/2004JA010413.

Borovsky, J. E., R. J. Nemzek, and R. D. Belian (1993), The occurrence rate of magnetospheric-substorm onsets: Random and periodic substorms, *J. Geophys. Res., 98*(A3), 3807-3814.

Boudouridis, A., E. Zesta, L.R. Lyons, P.C. Anderson, and D. Lummerzheim (2003), Effect of solar wind pressure pulses on the size and the strength of the auroral oval, *J. Geophys. Res., 108*(A4), 8012-8027, doi:10.1029/2002JA009373.

Chapman, S. and J. Bartels (1940), *Geomagnetism*, Oxford Clarendon Press.

Chua, D., G.Parks, M.Brittnacher, W. Peria, et al. (2001), Energy characteristics of auroral electron precipitation: A comparison of substorms and pressure pulse related auroral activity, *J. Geophys. Res., 106*(A4), 5945-5956.

Craven, J.D., J.S. Murphree, L.A. Frank, and L.L. Cogger (1991), Simultaneous optical observations of transpolar arcs in the two polar caps, *Geophys. Res. Lett., 18*(12), 2297-2300.

Cumnock, J.A., J.R. Sharber, R.A. Heelis, M.R. Hairston, and J.D. Craven (1997), Evolution of the global aurora during positive IMF Bz and varying IMF By conditions, *J. Geophys. Res., 102*(A8), 17489-17497.

Elphinstone, R.D., D. Hearn, J.S. Murphree, L.L. Cogger, M.L. Johnson, and H.B. Vo (1997), Some UV dayside auroral morphologies, in *Auroral Plasma Dynamics*, AGU Monograph, 31-45, American Geophysical Union, Washington D.C..

Friis-Christensen, E., Y. Kamide, A.D. Richmond, and S. Matsushita (1985), Interplanetary magnetic field control of high-latitude electric fields and currents determined from Greenland magnetometer data, *J. Geophys. Res., 90*, 1325-1338.

Friis-Christensen, E., M.A. McHenry, C.R. Clauer, and S. Vennerstrom (1988), Ionospheric traveling convection vortices observed near the polar cleft: a triggered response to sudden changes in the solar wind, *Geophys. Res. Lett., 15*, 253-256.

Iijima, T. and T.A. Potemra (1976), The amplitude distribution of field-aligned currents at northern high latitudes observed by Triad, *J. Geophys. Res., 81*, 2165.

Kamide, Y., W. Baumjohann, I.A. Daglis, W.D. Gonzales, et al. (1998), Current understanding of magnetic storm: Storm-substorm relationship, *J. Geophys. Res., 103*(A8), 17705-17728.

Knight, S. (1973), Parallel electric fields, {\it Planet. Space Sci., 21}, 741.

Koskinen, H.E.J., T.I. Pulkkinen, R.J. Pellinen, T. Bosinger, D.N. Baker, and R.E. Lopez (2002), Characteristics of pseudobreakups, in *Proceedings of the International Conference on Substorms (ICS-1), ESA SP-335*, 111-116.

Kremser, G., Woch, J., Mursula, K., Tanskanen, P., Wilken, B., and Lundin, R. (1995), Origin of energetic ions in the polar cusp inferred from ion composition measurements by the Viking satellite, *Ann. Geophys., 13,* 595.

Lopez,R.E., D.N.Baker, and J.Allen (2004), Sun Unleashes Halloween Storm, *Eos, 8*5, 105-108.

Lui, A.T.Y. (2004), Potential Plasma Instabilities For Substorm Expansion Onsets, *Space Sci. Rev., 113*, 127-206, doi: 10.1023/B:SPAC.0000042942.00362.4e.

Lui, A.T.Y., C. Jacquey, G.S. Lakhina, R. Lundin, et al. (2005), Critical Issues on Magnetic Reconnection in Space Plasmas, *Space Sci. Rev., 116*, 497-521.

Lyons, L.R., C.-P. Wang, and T. Nagai (2003), Substorm onset by plasma sheet divergence, *J. Geophys. Res., 108*(A12), 1427-1434, doi:10.1029/2003JA010178.

Lyons, L.R., and C.-P. Wang (2004), Fundamental aspect of substorm onset, *Proceedings of the 7th International Conference on Substorms*, edited by N. Ganushkina and T. Pulkkinen, 186-191, FMI, Helsinki.

Mende, S.B., H. Heetderks, H.U. Frey, M. Lampton, et al. (2000), Far ultraviolet imaging from the IMAGE spacecraft: 2. Wideband FUV imaging, *Space Sci. Rev., 91*, 271-285, doi:10.1023/A:1005227915363.

Meurant, M., J.-C. Gerald, B. Hubert, V. Coumans, et al. (2003), Dynamics of global scale electron and proton prcipitation induced by a solar wind pressure pulse, *Geophys. Res. Lett., 30*(20), 2032-2035, doi:10.1029/2003GL018017.

Morooka, M., T. Yamamoto, T. Mukai, K. Tsuruda, H. Hayakawa, and H. Fukunishi (1998), Relationship between field aligned currents and parallel electric field observed by Akebono, in *Substorm-4*, edited by S. Kokubun and Y. Kamide, 59–62, Terra Sci., Tokyo.

Nagai, T., S. and Machida (1998), Magnetic reconnection in the near-Earth magnetotail, in *New Perspectives on the Earth's Magnetotail*, edited by A. Nishida, D.N. Baker, and S.W.H. Cowley, AGU monograph, 211-224, American Geophysical Union, Washington D.C..

Ohtani, S., M. Nose, G. Rostoker, H. Singer, A.T.Y. Lui, and M. Nakamura (2001), Storm-substorm relationship: Contribution of the tail current to Dst, *J. Geophys. Res., 106*(A10), 21199-21209.

Ohtani, S. (2004), Flow Bursts in the Plasma Sheet and Auroral Substorm Onset: Observational Constraints on Connection Between Midtail and Near-earth Substorm Processes, *Space Sci. Rev., 113*, 77-96, doi: 10.1023/B:SPAC.0000042940.59358.2f.

Petrinec, S.M., K.Yumoto, H.Luhr, D.Orr, et al. (1996), The CME event of February 21, 1994: Response of the magnetic field at the Earth's surface, *J. Geomagn. Geoelectr., 48,* 1341.

Potemra, T.A., Sources of large-scale Birkeland currents (1994), in *Physical signatures of magnetospheric boundary layer process*, edited by J. A. Holtet, and A. Egeland, 3-27, Kluwer Academic Publishers, Dordrecht, Netherlands.

Sandholt, P.E., C.J., Farrugia, L.F. Burlaga, J.A. Holtet, et al. (1994), Cusp/cleft auroral activity in relation to solar wind dynamic pressure, interplanetary magnetic field B_Z and B_Y, *J. Geophys. Res., 99*, 17323.

Shue, J.-H. and Y. Kamide (1998), Effects of solar wind density on auroral electrojet, in *Substorm-4*, edited by S. Kokubun and Y. Kamide, 677-680.

Stenbaek-Nielsen, H.C. and A. Otto (1997), Conjugate auroras and the interplanetary magnetic field *J. Geophys. Res. 102*(A2), 2223-2232.

Tsyganenko, N.A. (1995), Modeling the Earth's Magnetospheric Magnetic Field Confined Within a Realistic Magnetopause, *J. Geophys. Res., 100*, 5599-5612.

Tsyganenko, N.A. and D.P. Stern (1996), A new generation global magnetosphere field model, based on spacecraft magnetometer data, *ISTP newsletter, 6*, No.1, 21.

Tsyganenko, N.A., Geopack-2003 (2003), http://modelweb.gsfc.nasa.gov/magnetos/data-based/Geopack_2003.html

Woch, J., M. Yamauchi, R. Lundin, T.A. Potemra, and L.J. Zanetti (1993), The low-latitude boundary layer at mid-altitudes: Relation to large-scale Birkeland currents, *Geophys. Res. Lett., 20*, 2251-2254.

Zesta, E., H.J. Singer, D. Lummerzheim, C.T. Russell, L.R. Lyons, and M.J. Britnacher (2000), The effect of the January 10, 1997, Pressure pulse on the magnetosphere-ionosphere current system, in *Mangetospheric Current System*, edited by S. Ohtani, R. Fujii, M. Hesse, and R.L. Lysak, AGU monograph, 217-226, American Geophysical Union, Washington D.C..

Zhou, X. and B.T. Tsurutani (1999), Rapid intensification and propagation of the dayside aurora: Large scale interplanetary pressure pulses (fast shock), *Geophys. Res. Lett., 26*(8), 1097-1100.

Zhou, X.-Y., R. J. Strangeway, P. C. Anderson, D. G. Sibeck, et al. (2003), Shock aurora: FAST and DMSP observations, *J. Geophys. Res., 108*(A4), 8019, doi:10.1029/2002JA009701.

H. Frey, Space Science Laboratory, University of California, Berkeley, CA 94720-7450, USA. (hfrey@ssl.berkeley.edu)

M. Henderson, Los Alamos National Lab, P.O. Box 1663, Los Alamos, NM 87545, USA. (mghenderson@lanl.gov)

T. Iyemori, Data Analysis Center C2 for Geomagnetism and Space Magnetism, Kyoto University, Kyoto 606-8502, Japan. (iyemori@kugi.kyoto-u.ac.jp)

M. Yamauchi, Swedish Institute of Space Physics, Box 812, SE-98128 Kiruna, Sweden. (M.Yamauchi@irf.se)

Figure Captions

Figure 1: Provisional geomagnetic indices for the 2003-10-29 magnetic storm. (a) Dst index, (b) AE index, (c) SYM and ASY indices.

Figure 2: Interplanetary magnetic field data observed before and after the strong interplanetary shock that caused the sudden commencement of the geomagnetic storm at around 06:10 UT on 2003-10-29. (a) ACE spacecraft (221 R_E upstream) with 16-seconds resolution, (b) Geotail spacecraft (26 R_E upstream) with 1-second resolution.

Figure 3: Energetic particle data from the SOPA instrument on board the LANL geosynchronous satellites during the initial phase of the 2003-10-29 storm (06:00-06:30 UT). (a) Proton flux (50-400 keV); (b) Electron flux (50-300 keV). The local times of the satellites at 06 UT are, from top to bottom, 07 LT (LANL-01A), 11 LT (LANL-02A), 13 LT (LANL-97A), 16 LT (1994-084), 19 LT (1991-080), and 04 LT (1990-095).

Figure 4: Magnetic field data (5s resolution) from geosynchronous GOES-10 at around 21 LT (thin lines) and GOES-12 at around 01 LT (think lines) during the initial phase of the 2003-10-29 storm (06:10-06:20 UT). H_P is northward component perpendicular to the spin plane (nearly parallel to the Earth's spin axis); H_E is Earthward component perpendicular to H_P; H_N is eastward component completing local Cartesian coordinate; |B| is total field; inc = atan(H_P/H_E); and dip = acos(H_P/|B|). Magnetic field data from Polar (6s resolution), which was located only 1 R_E away from GOES-10 at 21 LT, is over-plotted with broken lines in the SM coordinate system (Hp: parallel to Earth's dipole axis and 11° off from Earth's spin axis). The vertical dot-dash-lines (06:11:40 UT and 06:16:40 UT) indicate the arrival time of the shock and the onset timing of the very localized 4000 nT activity at the ground (see section 3.1), respectively.

Figure 5: Deviation in the horizontal component on 2003-10-29 at 06:11:10-06:11:30 UT. From top to bottom, ΔX component at Kiruna (07 LT, 65° GMLat), ΔH components of Urumqi (12 LT, 34° GMLat), Memanmetsu (16 LT, 35° GMLat), and Kanoya (15 LT, 22° GMLat).

Figure 6: Illustration of the spacecraft locations viewed from the north (except Cluster) at around 6 UT on 2003-10-29 when the interplanetary shock passed the Earth. Shock was registered in the magnetometer data of ACE, Geotail (GTL: 1s resolution), and Wind spacecraft in the solar wind and Cluster (CL), Polar (PLR), GOES (G) satellites inside the magnetosphere. The energetic particles data by LANL satellites, i.e., LANL-01A (L-1A), LANL-02A (L-2A), LANL-97A (L-97), 1994-084 (1994), 1991-080 (1991), and 1990-095 (1990) also show the shock arrival. Time resolution is 10s or better except for ACE (16s resolution).

Figure 7: Worldwide geomagnetic field on 2003-10-29 at 06-07 UT: (a) in the auroral zone (GMLat ≈ 65°); (b) in the sub-auroral region (GMLat < 63°); (c) in the high latitude side of the auroral zone (GMLat > 70°).

Figure 8: IMAGE-FUV data in the magnetic coordinate (GMLat and MLT) at 06:11-06:18 UT on 2003-10-29 taken from the southern hemisphere: (a) at around 06:11:40 UT; (b) at around 06:13:40 UT; (c) at around 06:15:40 UT; (d) at around 06:17:40 UT.

Figure 9: Illustration of the basic dayside current system looking from the night toward the sun. While Region 1 field-aligned current normally comes from magnetospheric boundary (plasma sheet boundary for the nightside case), Region 2 field-aligned current normally comes from the plasma sheet and the ring current. Ionospheric Pedersen current closes this current system, and corresponding electric field causes the Hall current which is the major contributor to both the ionospheric current (electrojet) and the ground geomagnetic signature. Region 1 and Region 2 field-aligned currents in the dawn/dusk sectors are topologically symmetric between the hemispheres although their intensity and exact locations can be different. The aurora in the dawn/dusk sectors normally corresponds to upward current where keV electrons flow downward, and is normally topologically symmetric between the conjugate hemispheres.

Table 1. Time sequence during the first 8 minutes of SC in 10-seconds resolution

UT	Magnetosphere	Ground ΔB	Image
06:09:40	Shock arrival at X=26 R_E upstream.		
0610:50	Shock arrival at LANL-02A (11 LT) and LANL-97A (13 LT).		
0611:10	Shock arrival at LANL-01A (7 LT).		
0611:20	Shock arrival at 1990-095 (4 LT), 1994-084 (16 LT), and Cluster (X=0 R_E, Z=-10 R_E).		
0611:20		Start of SC.	
0611:30			Residual from the previous auroral arc.
0611:30	Shock arrival at 1991-080 (19 LT) and Polar (21 LT, Z=0 R_E).		
0611:40	Shock arrival at GOES-12 (1 LT) and GOES-10 (21 LT).		
0612:00	Start of dipolarization at GOES-12 (1 LT).		
0612		Peak of SC.	
0612		Onset of westward electrojet in evening-midnight.	
0612:20	End of dipolarization at GOES-12 (1 LT).		
0612:20	More stretched B-field than at the shock arrive GOES-10 (21 LT).		
0612:20	Short spike of E~20 mV/m at Polar.		
0612 ~ 0613		Onset of westward electrojet in morning.	
0613:00	Start of cross-tail current decrease with E-field increase at 21 LT (Polar and GOES-10).		
0613		ΔB<-1000 nT at CMO (20 LT).	
0613:30			Sudden intensification of midnight spot and morning arc.
0614:00	Peak of E (=40~50 mV/m) at Polar.		
0615		ΔB<-2000 nT at LRV (4 LT).	
0615:40			Expansion of midnight brightening (poleward) and

			morning brightening (westward).
0616		ΔB<-2000 nT at YKC (22 LT) and PBQ (1 LT).	
0616:40	Sharp spike of B at GOES-12 (1 LT).		
0617		Onset of ΔBx<0 at IQA (1 LT).	
0617:40			Two brightened regions merged at post-midnight.
0618		ΔBx = -3000 nT/min at IQA (1 LT).	

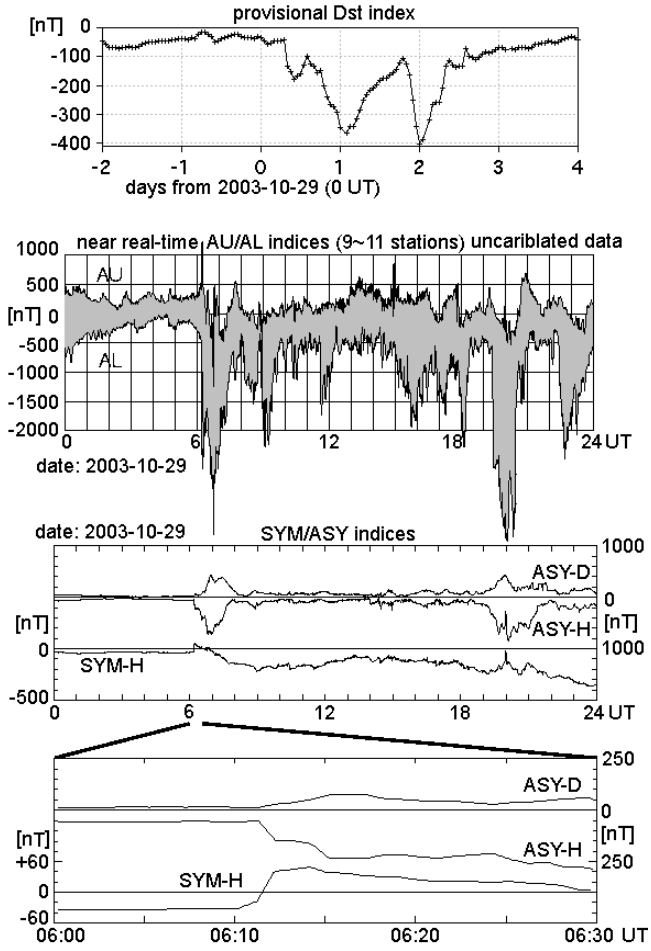

Figure 1: Provisional geomagnetic indices for the 2003-10-29 magnetic storm. (a) Dst index, (b) AE index, (c) SYM and ASY indices.

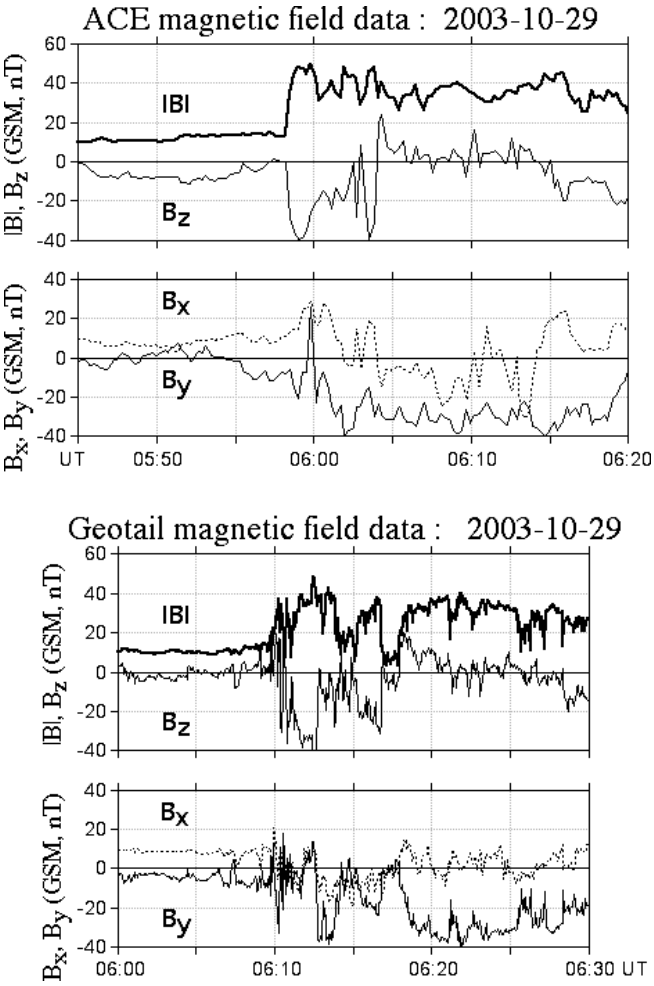

Figure 2: Interplanetary magnetic field data observed before and after the strong interplanetary shock that caused the sudden commencement of the geomagnetic storm at around 06:10 UT on 2003-10-29. (a) ACE spacecraft (221 R_E upstream) with 16-seconds resolution, (b) Geotail spacecraft (26 R_E upstream) with 1-second resolution.

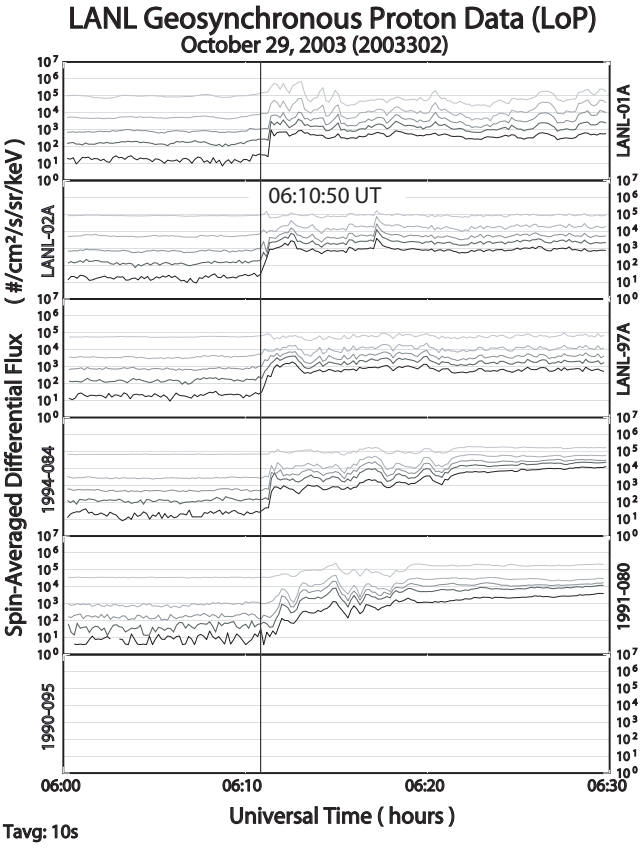

Figure 3: Energetic particle data from the SOPA instrument on board the LANL geosynchronous satellites during the initial phase of the 2003-10-29 storm (06:00-06:30 UT). (a) Proton flux (50-400 keV); (b) Electron flux (50-300 keV). The local times of the satellites at 06 UT are, from top to bottom, 07 LT (LANL-01A), 11 LT (LANL-02A), 13 LT (LANL-97A), 16 LT (1994-084), 19 LT (1991-080), and 04 LT (1990-095).

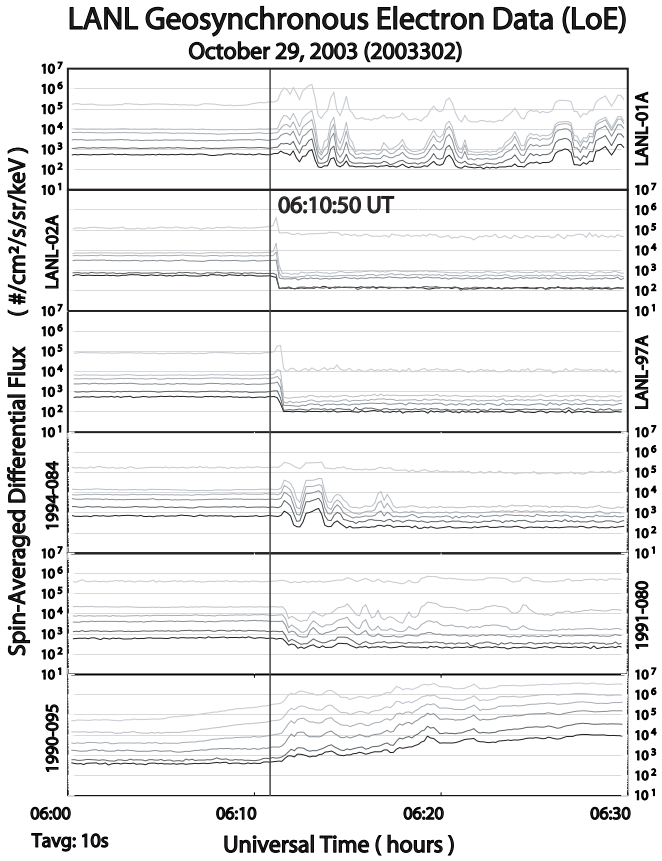
LANL Geosynchronous Electron Data (LoE)
October 29, 2003 (2003302)
Spin-Averaged Differential Flux (#/cm²/s/sr/keV)
06:10:50 UT
LANL-01A
LANL-02A
LANL-97A
1994-084
1991-080
1990-095
06:00
06:10
06:20
06:30
Tavg: 10s
Universal Time (hours)

Figure 3b

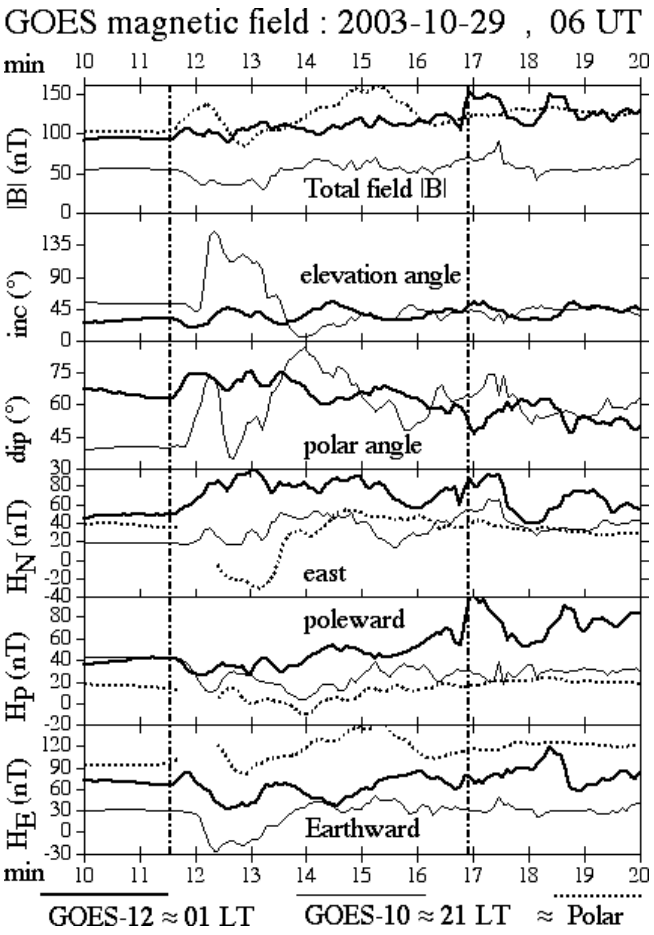

Figure 4: Magnetic field data (5s resolution) from geosynchronous GOES-10 at around 21 LT (thin lines) and GOES-12 at around 01 LT (think lines) during the initial phase of the 2003-10-29 storm (06:10-06:20 UT). H_P is northward component perpendicular to the spin plane (nearly parallel to the Earth's spin axis); H_E is Earthward component perpendicular to H_P; H_N is eastward component completing local Cartesian coordinate; |B| is total field; inc = atan(H_P/H_E); and dip = acos(H_P/|B|). Magnetic field data from Polar (6s resolution), which was located only 1 R_E away from GOES-10 at 21 LT, is over-plotted with broken lines in the SM coordinate system (Hp: parallel to Earth's dipole axis and 11° off from Earth's spin axis). The vertical dot-dash-lines (06:11:40 UT and 06:16:40 UT) indicate the arrival time of the shock and the onset timing of the very localized 4000 nT activity at the ground (see section 3.1), respectively.

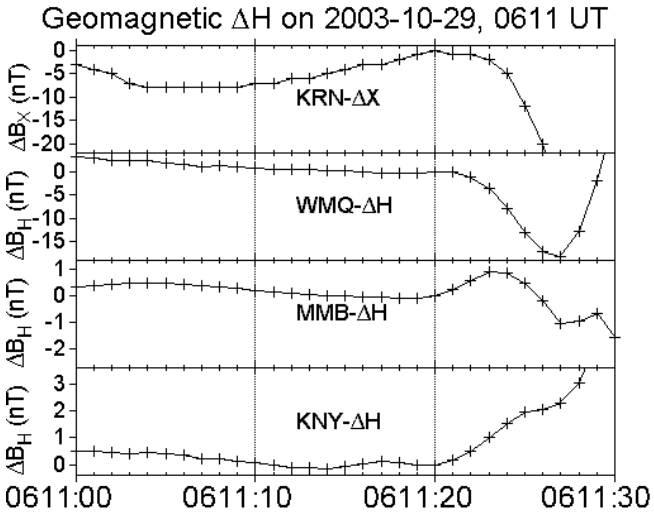

Figure 5: Deviation in the horizontal component on 2003-10-29 at 06:11:10-06:11:30 UT. From top to bottom, ΔX component at Kiruna (07 LT, 65° GMLat), ΔH components of Urumqi (12 LT, 34° GMLat), Memanmetsu (16 LT, 35° GMLat), and Kanoya (15 LT, 22° GMLat).

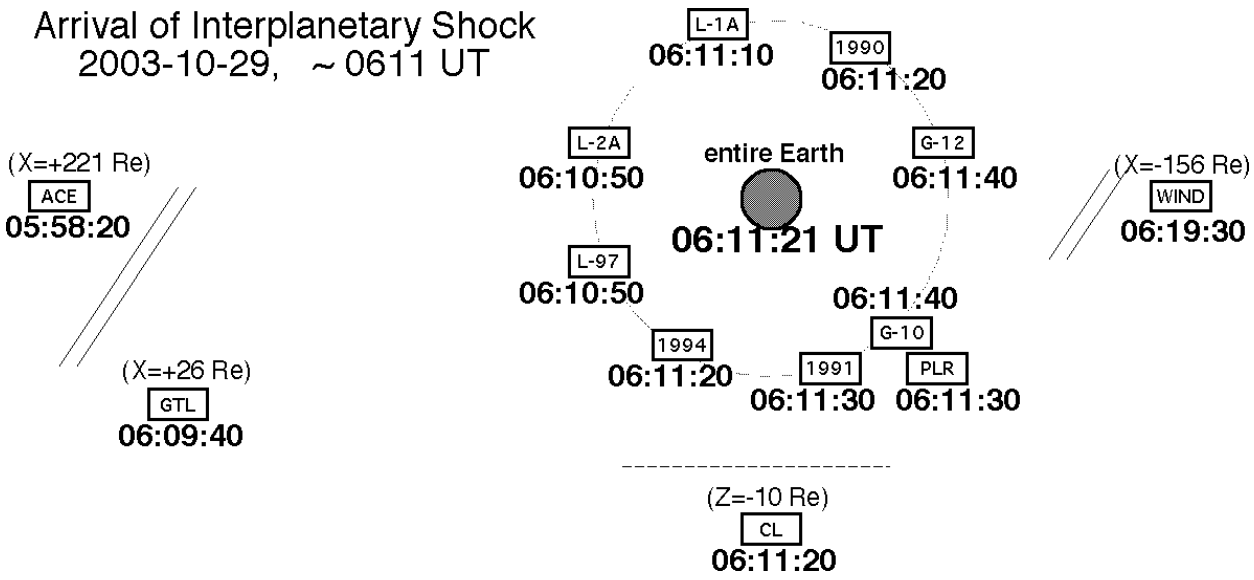

Figure 6: Illustration of the spacecraft locations viewed from the north (except Cluster) at around 6 UT on 2003-10-29 when the interplanetary shock passed the Earth. Shock was registered in the magnetometer data of ACE, Geotail (GTL: 1s resolution), and Wind spacecraft in the solar wind and Cluster (CL), Polar (PLR), GOES (G) satellites inside the magnetosphere. The energetic particles data by LANL satellites, i.e., LANL-01A (L-1A), LANL-02A (L-2A), LANL-97A (L-97), 1994-084 (1994), 1991-080 (1991), and 1990-095 (1990) also show the shock arrival. Time resolution is 10s or better except for ACE (16s resolution).

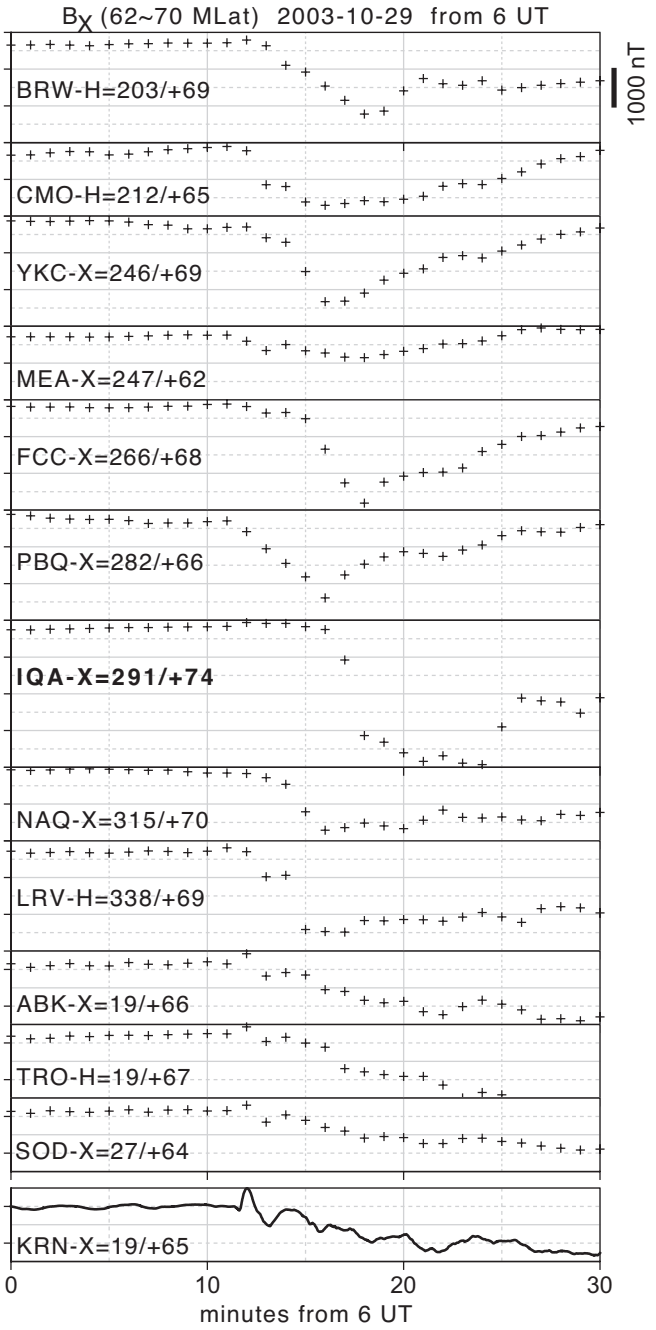

Figure 7: Worldwide geomagnetic field on 2003-10-29 at 06-07 UT: (a) in the auroral zone (GMLat ≈ 65°); (b) in the sub-auroral region (GMLat < 63°); (c) in the high latitude side of the auroral zone (GMLat > 70°).

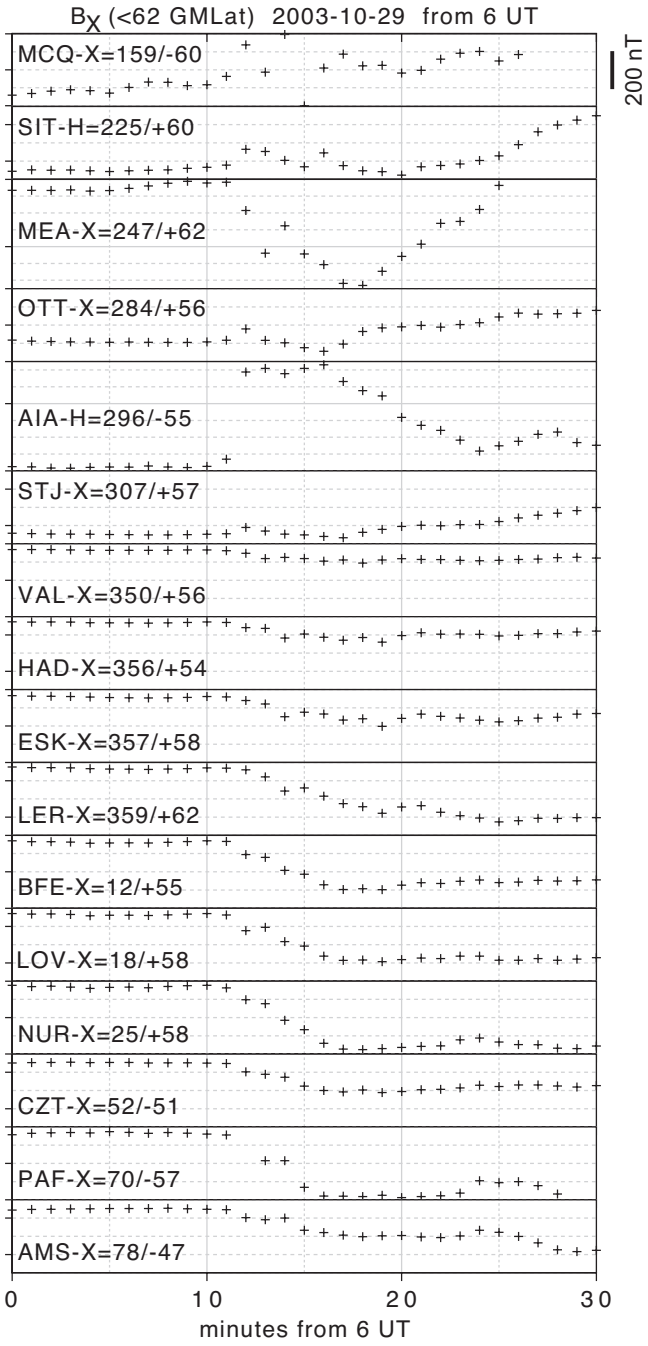
B_X (<62 GMLat) 2003-10-29 from 6 UT
200 nT
MCQ-X=159/-60
SIT-H=225/+60
MEA-X=247/+62
OTT-X=284/+56
AIA-H=296/-55
STJ-X=307/+57
VAL-X=350/+56
HAD-X=356/+54
ESK-X=357/+58
LER-X=359/+62
BFE-X=12/+55
LOV-X=18/+58
NUR-X=25/+58
CZT-X=52/-51
PAF-X=70/-57
AMS-X=78/-47
0
10
20
30
minutes from 6 UT

Figure 7b

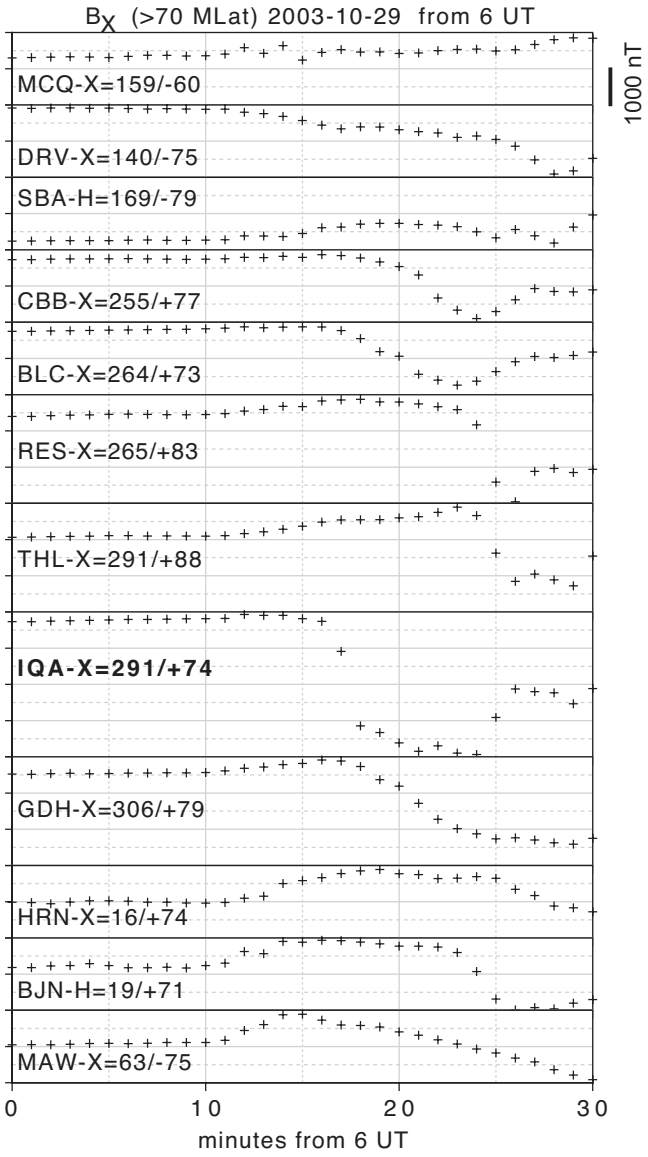
B_X (>70 MLat) 2003-10-29 from 6 UT
1000 nT
MCQ-X=159/-60
DRV-X=140/-75
SBA-H=169/-79
CBB-X=255/+77
BLC-X=264/+73
RES-X=265/+83
THL-X=291/+88
IQA-X=291/+74
GDH-X=306/+79
HRN-X=16/+74
BJN-H=19/+71
MAW-X=63/-75
0
10
20
30
minutes from 6 UT

Figure 7c

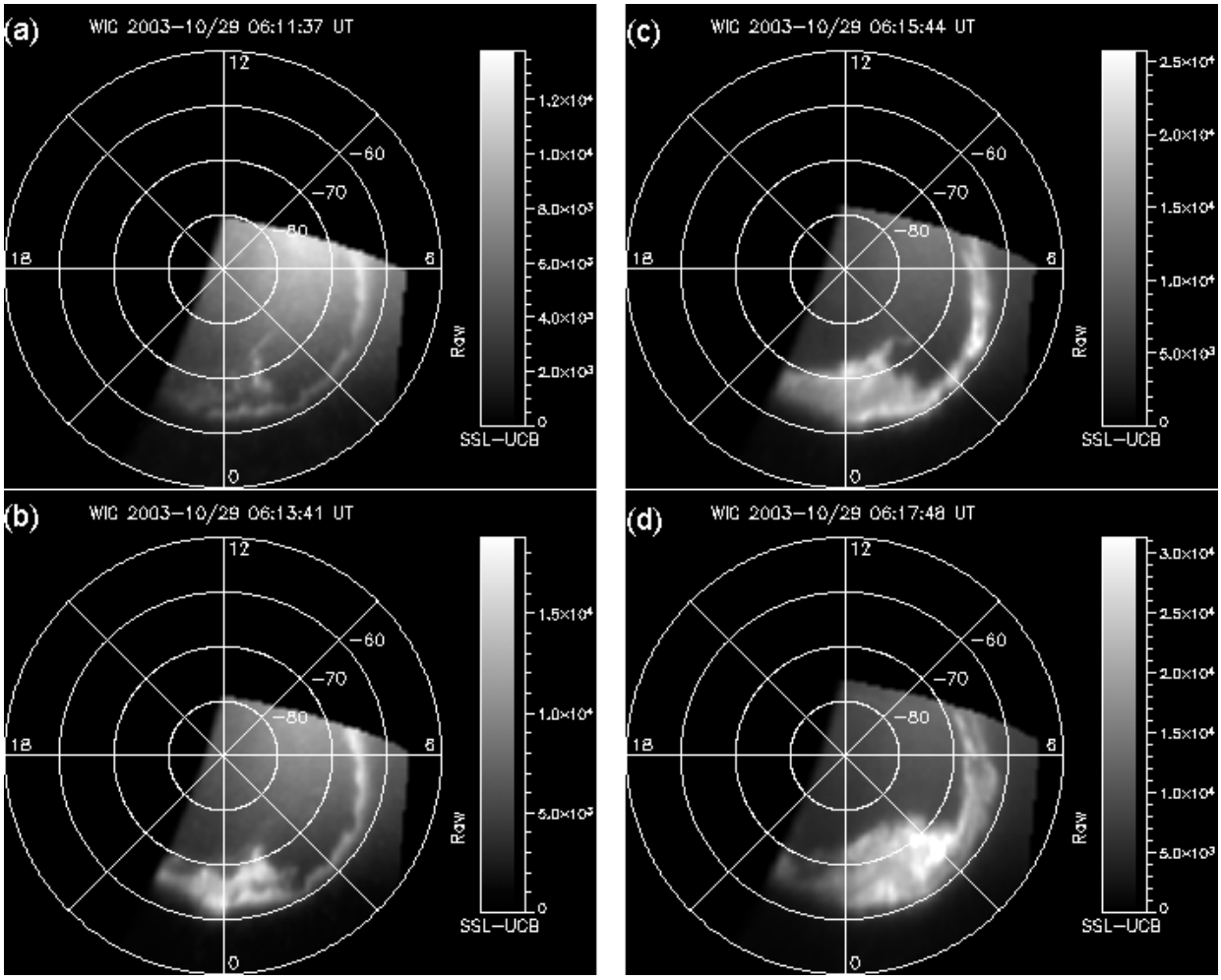

Figure 8: IMAGE-FUV data in the magnetic coordinate (GMLat and MLT) at 06:11-06:18 UT on 2003-10-29 taken from the southern hemisphere: (a) at around 06:11:40 UT; (b) at around 06:13:40 UT; (c) at around 06:15:40 UT; (d) at around 06:17:40 UT.

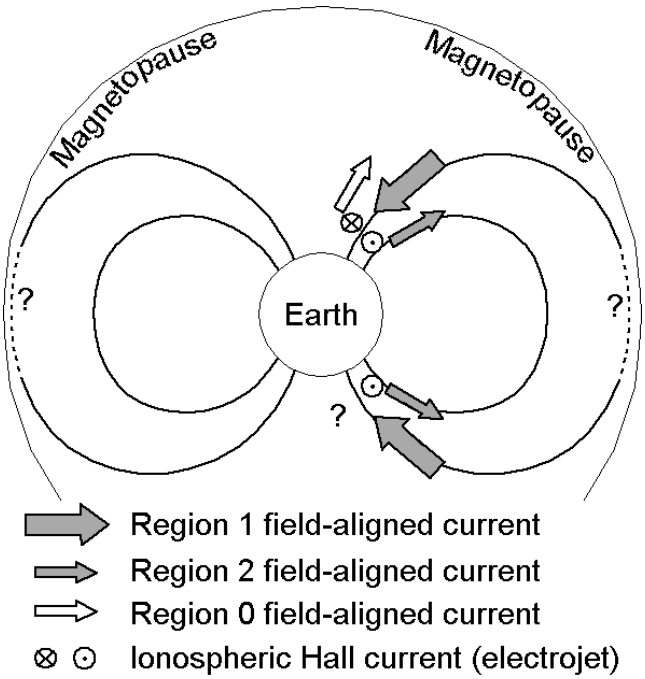

Figure 9: Illustration of the basic dayside current system looking from the night toward the sun. While Region 1 field-aligned current normally comes from magnetospheric boundary (plasma sheet boundary for the nightside case), Region 2 field-aligned current normally comes from the plasma sheet and the ring current. Ionospheric Pedersen current closes this current system, and corresponding electric field causes the Hall current which is the major contributor to both the ionospheric current (electrojet) and the ground geomagnetic signature. Region 1 and Region 2 field-aligned currents in the dawn/dusk sectors are topologically symmetric between the hemispheres although their intensity and exact locations can be different. The aurora in the dawn/dusk sectors normally corresponds to upward current where keV electrons flow downward, and is normally topologically symmetric between the conjugate hemispheres.